NOLTR 66-70

HYDRODYNAMIC PRESSURE MEASUREMENTS OF THE VERTICAL WATER ENTRY OF A SPHERE

26 OCTOBER 1966

NOL

UNITED STATES NAVAL ORDNANCE LABORATORY, WHITE OAK, MARYLAND

NOLTR 66-70

Distribution of this document is unlimited.

Ballistics Research Report 161

HYDRODYNAMIC PRESSURE MEASUREMENTS OF THE VERTICAL WATER ENTRY OF A SPHERE

Prepared by:

W. R. Hoover and V. C. D. Dawson

ABSTRACT: The phenomena associated with the vertical water entry of 2-inch-diameter aluminum spheres striking the water surface at 28 feet per second have been investigated by the use of hydrophones placed below the water surface.

The pressure recordings from the hydrophones have been analyzed for the three distinct phases of the water-entry problem: namely, (1) impact phase, (2) cavity flow phase, and (3) cavity collapse.

The impact phase has been analyzed by means of a dipole theory and a momentum equation. These have been compared to the results of other theoretical and experimental investigators and the actual pressure as measured at a point in the fluid. The comparison of measured and calculated pressures is not very good during this initial phase of water entry. The acceleration acting on the body as computed by the momentum equation agrees well with the results of other experimental and theoretical investigators.

The cavity flow phase was analyzed by the potential theory of a half-body placed in a uniform flow since the shape of the water-entry cavity is very similar to a half-body. A comparison of actual pressures recorded with those as predicted by the half-body theory show agreement within ten percent both outside and inside the cavity.

U. S. NAVAL ORDNANCE LABORATORY
WHITE OAK, MARYLAND

NOLTR 66-70 26 October 1966

HYDRODYNAMIC PRESSURE MEASUREMENTS OF THE VERTICAL WATER ENTRY OF A SPHERE

The material presented in this report was the outcome of the conception that the axial force acting on a missile during its water-entry phase could be related to the acoustic pressure measured at some point in the water. The usefulness of such an idea would be of tremendous value in the design of water-entry missiles.

This problem is one of great complexity, due mainly to the transient nature of the phenomenon of water entry.

E. F. SCHREITER
Captain, USN
Commander

A. E. Seigel
A. E. SEIGEL
By direction

CONTENTS

CONTENTS (Cont'd)

ILLUSTRATIONS

LIST OF SYMBOLS

A	maximum cross-sectional area of the sphere, or amplitude of the complex velocity potential (when applicable)
a	radius of the vibrating sphere, or change of radius of the oscillating sphere (when applicable)
c	speed of sound in water
C_D	drag coefficient
C	constant in the velocity potential of a dipole
C_o	capacitance of filter circuit
C_S	speed of sound in the sphere
cm	centimeter
f	frequency of vibration
F	force on the missile
k	ratio of specific heats of a gas, or wave number, n/c (when applicable)
m	mass of sphere
ms	millisecond
mv	millivolt
n	circular frequency of vibration of the sphere
p	pressure
q	total velocity of the fluid at a point, or charge on capacitor in filter circuit (when applicable)
r	distance between point of impact of sphere to pressure pickup gage in water
R_o	resistance in filter circuit
ρ	density of water
T	period of oscillation

LIST OF SYMBOLS (Cont'd)

t	time
μs	microsecond
V,U	velocity of sphere, or water velocity at infinity (when applicable)
x	radius of circle that is the intersection between the sphere and the plane water surface
y	depth of submergence of the sphere below the water surface
σ	Poisson's ratio
λ	wave length
θ	directional angle to a point
Φ	velocity potential
Ψ	stream function

INTRODUCTION

It is well known that missiles entering water produce sounds both in the air and beneath the water surface. The dripping of a faucet onto a pail of water is probably the most common example of this complex phenomenon. More than sixty years ago Worthington, reference (1), used single-spark photography to discover the cavity which followed the entry of droplets and spheres into water. His excellent photographic study showed qualitatively the splash, surface seal of the cavity, cavity closure, formation of re-entrant jets, and many other details associated with the water entry of spheres, both free fall and propelled from an air gun into water. More than forty years ago Mallock, reference (2), repeated some of the experiments of Worthington and gave a tentative explanation of the shapes of the cavities produced. Since the sounds produced by the water-impact, when observed in air, were similar to a musical character, Mallock attributed them to the vibration of the cavity formed behind the impinging missile. About 1933, Minnaert, reference (3), explained the origin of underwater sound by bubbles and determined the resonant frequency of a bubble in volume pulsation for a reversible adiabatic (isentropic) process. Milne-Thomson, reference (4), gives essentially the same relationship for an isothermal process where the pressure in the spherical cavity does not deviate too much from the surrounding pressure of the fluid. The original work of Worthington was repeated and extended with more modern equipment by Richardson, references (5) and (6), and May, reference (7). Richardson concluded that at the instant of cavity closure the steady state of the cavity could be represented by a potential flow due to a source together with a linear sink of the same total strength stretching from the source vertically up to some distant point from the closure. Although the deceleration which the sphere is actually experiencing is ignored, the potential solution is a good approximation to the field of flow in this pseudo-steady case. Despite the rather crude instrumentation, Richardson found that the pressure in the cavity remained nearly atmospheric until the cavity closed. As the cavity closed, large oscillations of the pressure in the cavity supervened but were rapidly damped and rose in frequency with time. He concluded that the underwater sound was mainly due to damped pulsations of volume excited by collapse of the cavity or its parts. May was mainly concerned with the scaling of cavities formed when spheres entered water. He found that Froude scaling was a good first approximation in describing cavity behavior and that some improvement is effected by the pressure-density scaling of the atmosphere above the water. The energy lost by a missile during the

open-cavity phase of its water entry was found to be used up principally in the formation of the cavity. For a given drag force the cavity shape after water entry was found to be independent of the nose shape of the missile.

Present Problem. This report had its conception in the idea that the axial force on a missile entering water vertically could somehow be related to the pressure measured at some point in the fluid. A phase shift would be evident due to the finite speed of sound in the fluid, but the advantages of using such a system to monitor the water-entry forces on missiles would be of paramount importance. No physical contact with the missile of any type of instrumental equipment would be required. Accelerometers placed in the water-entry missile require either internal recording, trailing cables, or radiotelemetry to transmit the data from the accelerometer and store it by some means. Besides many other disadvantages the above items are either costly or limited to low-entry velocities. By using the pressure measuring technique of determining water-entry forces, no special models or launching guns would be required. Pressure measurements could be taken conveniently anywhere in the fluid and could be directly recorded on fast writing, quick response oscilloscopes. Triggering the recording scope would be no problem since another pressure gage could be used as a signalling device to the scope, set at a distance away from the pressure pickup gage such that a sufficient length of zero base line would be recorded.

Since the pressure gage would already be in the water, it would be of interest to continue the pressure signal monitoring and record the entire pressure at the gage due to the history of the cavity developed by the model.

DESCRIPTION OF THE WATER-ENTRY PHENOMENA OF A SPHERE

Impact and Missile Oscillation

This is defined to be the stage of water entry where the highest force on the missile is generated, and, hence, in the time domain of highest pressures on the nose of the missile. The order of magnitude of the time required for the missile to experience the maximum water-entry force is generally found to be the time required for the missile to travel one-tenth of its radius at the constant water-entry velocity. During this time, there is no separation of the water flow

from the nose of the missile; i.e., there is complete contact between the surface of the sphere that has pierced the water surface and the water itself. If the missile has rigidity and a high enough natural frequency, forced vibration of the missile may start at this time and continue until the natural damping nullifies the oscillations.

Open Cavity Flow

After the impact phase just described, the water flow around the sphere separates at approximately 67 degrees up from the initial contact point. It is at this time that the cavity is formed behind the sphere. As the cavity grows larger and longer, the top of the cavity will dome over to seal the lower portion from the atmosphere. This is caused by the water which splashed up from the original water surface. At this time, the cavity is closed to the atmosphere. As the missile continues to move on its trajectory, the volume of the cavity expands and the pressure in the cavity is relieved due to this expansion. The pressure in the cavity may vary considerably from one part of the cavity to another.

Cavity Collapse and Cavity Oscillation

The diameter at any cavity cross section will reach its maximum dimension when the energy given to a unit layer of water by the missile equals the work done in expanding the cavity against the hydrostatic pressure at that cross section. After this time, the diameter will decrease principally due to the difference in pressure between that in the cavity and the hydrostatic head. This decrease of the diameter is what is called cavity collapse. The cavity collapse may be generally categorized in three distinct types; namely, point closures, line closures, and base closures, reference (8). The cavity diameters will decrease in some fashion resembling the outline of an hourglass. At the waist of the hourglass figure of the cavity, the cavity will pinch off into two separate cavities. The upper section of the cavity will move toward the surface of the water while the lower portion of the cavity will move toward the model, thus forming a closed, slender cavity trailing the model. Sometimes, instead of the cavity closing at a point in the hourglass fashion, closure of the cavity will take place almost simultaneously over a large length of the cavity. This type of cavity collapse is called a line closure. A lower entrance velocity of the missile is required to obtain the line closure of the cavity

as compared to the point closure. The third type of cavity collapse, the base closure, occurs at still lower entrance velocities than the line closure. The base closure seems to be the most common type of cavity closure observed. The ase closure represents an acceleration of the rear of the cavity from the surface of the water to the missile. The above three types of cavity closure can generally be found for any one missile by varying the entrance velocity. If the initial velocity of the entering missile is held constant, the three types of cavity closure can be obtained generally by varying the weight of the missile.

After the deep closure of the cavity takes place, whether line, point, or base closure, the cavity will oscillate in volume due to the transient nature of the closed cavity phenomenon. The pulsations of the air-filled cavity that is formed in the water are usually more severe than the shock wave that is propagated through the water on entry impact.

DESCRIPTION OF TEST FACILITY AND INSTRUMENTATION

The experimental equipment required to obtain pressure information at a point in the water due to a model entering the water can be extremely simple. The electronic problems associated with such a test setup may prove to be extremely troublesome.

The test equipment and procedure as used in this report may be described in the following manner.

Two-inch-diameter aluminum spheres were dropped vertically through a five-foot section of 2-1/4-inch I.D. glass tubing onto a water surface. The glass tubing served as a guide and was aligned in two planes by means of an air-bubble level so that its axis would be perpendicular to the water surface. The water surface was contained in a glass-walled, rectangular tank, approximately 20 feet long by 5 feet wide and 9 feet deep. The free-fall drop height of the spheres was approximately 13 feet. A brass rod mounted at the center of the tank and protruding through the water surface served as a positioning mounting for two hydrophones. The lower hydrophone was the pressure pickup transducer that recorded all pressure signatures. The hydrophone above the pressure pickup served as a triggering device for the recording oscilloscope. The axis of the pickup hydrophone was normal to the trajectory of the

dropped spheres. The triggering hydrophone located approximately four inches above the pickup hydrophone and parallel to it was rotated approximately 60 degrees with respect to the pickup hydrophone so that its interference with the pressure wave to be measured would be negligible. Interference of the pressure wave will occur and has been measured when the hydrophones are improperly placed. Below the hydrophones and on the floor of the tank were placed a nylon rope impact mat and a turkey-wire catch basket. The nylon impact mat prevented the spheres from damaging the protective coating on the steel floor of the tank. The catch basket retained the spheres on the bottom of the tank and was raised to the first story floor by means of a retrieving nylon rope whenever the supply of spheres was exhausted.

Placement of the pickup hydrophone was achieved by means of a plumb line dropped through the center of the glass guide tube. This hydrophone was generally located 12 inches below the surface of the water and 6 inches to one side of the sphere's straight line trajectory.

The pickup hydrophone was fed into an impedance matching device (cathode follower) when necessary, then into the operational filter (when used), and finally into the vertical amplifier of the recording oscilloscope. The oscilloscope trace was photographed with a Polaroid camera attached to the oscilloscope CRT. The triggering hydrophone was fed into the vertical amplifier of another oscilloscope. The "plus gate out" of this oscilloscope was then used to give a signal to sweep the recording oscilloscope. By this means various triggering signal levels could be achieved to trigger the recording oscilloscope.

To photographically record the water entry and cavity phenomena, a Fastax high-speed camera was used, operating at approximately 1,000 frames per second. Timing marks of 500 cycles per second were placed on one edge of the film as it advanced through the camera, thus giving an accurate indication of the instantaneous framing rate of the camera. Since the water-entry tank was placed in a relatively narrow room, a front-surface mirro was used to effectively increase the optical path between the water-entry events and the high-speed camera. This permitted a sufficiently large image to be obtained on the photographic motion picture film without optical distortion taking place.

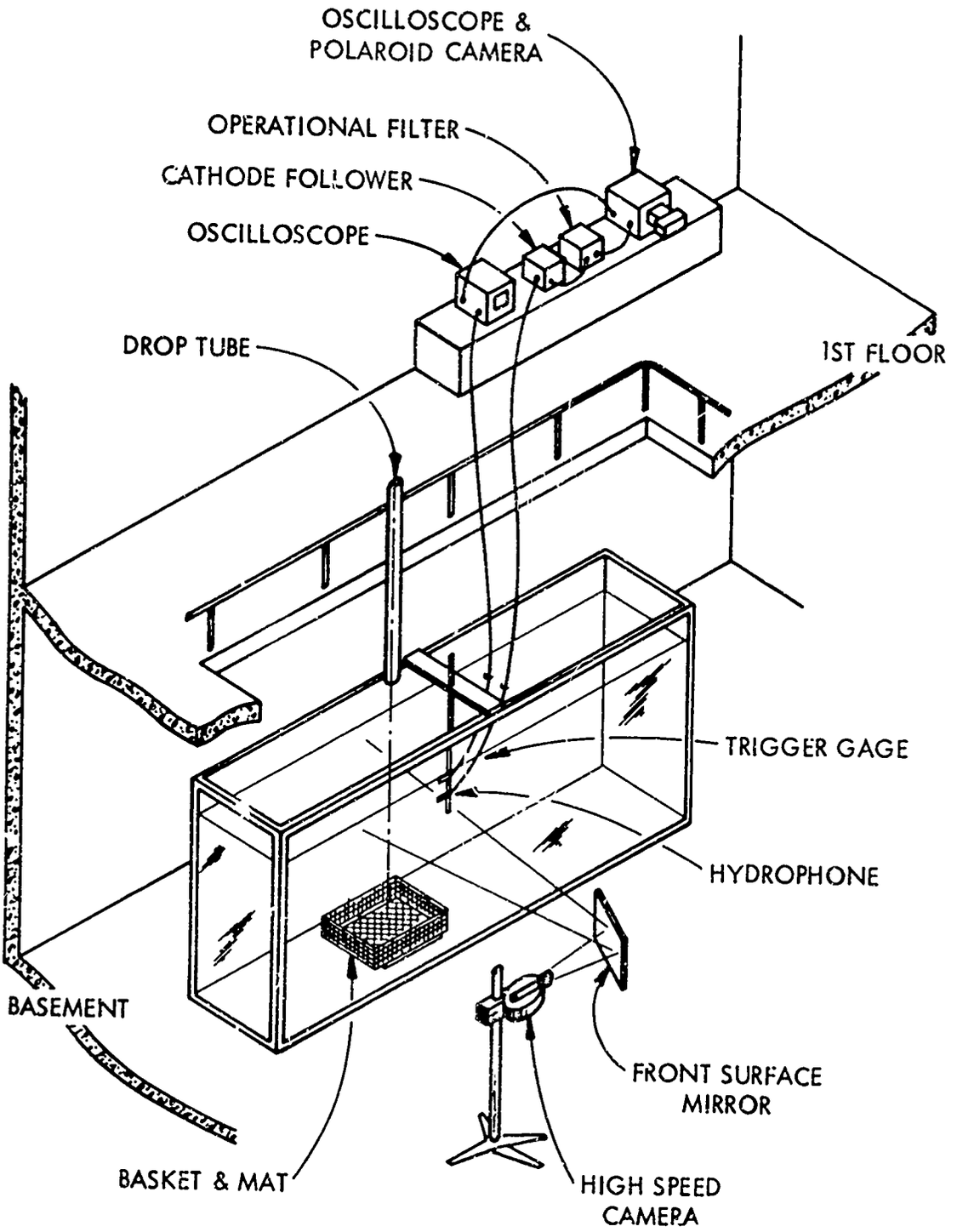

TEST EQUIPMENT SCHEMATIC

EQUIPMENT AND INSTRUMENTATION

Tap Water

Tank, 20 feet x 5 feet x 9 feet deep

2-inch-diameter aluminum alloy 6061 ST6 spheres

Pressure transducer hydrophone, Model LC-10, lead zirconate titanate sensing element, with low noise cable manufactured by Atlantic Research Corporation, Alexandria, Virginia

Oscilloscope, Model 1805, with a 0.01 μs rise time, Model 1824 High Gain Differential Preamplifier, manufactured by Hickok Electrical Instrument Company, Cleveland, Ohio

Oscilloscope, Type 561 A, with a 0.10 μs rise time type 2A63 Differential Amplifier, manufactured by Tektronix, Inc., Portland, Oregon

Oscilloscope Polaroid Camera, Model C-12, manufactured by the Tektronix, Inc., Portland, Oregon

Fastax High-Speed Camera, variable speed, manufactured by the Wollensak Division of Revere Camera (Division of the 3M Co.) Rochester, New York

Extraneous paraphernalia such as: impact mat, catch basket, retrieving rope, front surface mirror, mounting rods, glass guide tube, cathode follower, operational filters, and coaxial hookup cables

THEORETICAL AND EXPERIMENTAL ANALYSIS

Impact Phase

Figure 1 shows a typical oscilloscope recording of the impact pressure, as seen by the crystal pressure gage, produced by a 2-inch-diameter aluminum sphere entering the water surface normally at 28 feet per second. The pressure gage was located approximately four inches below the water surface and four inches from the straight line trajectory of the sphere.

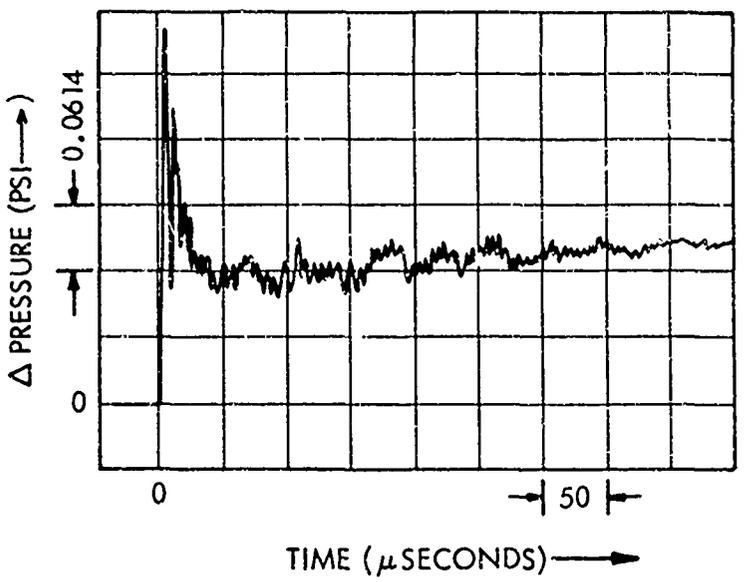

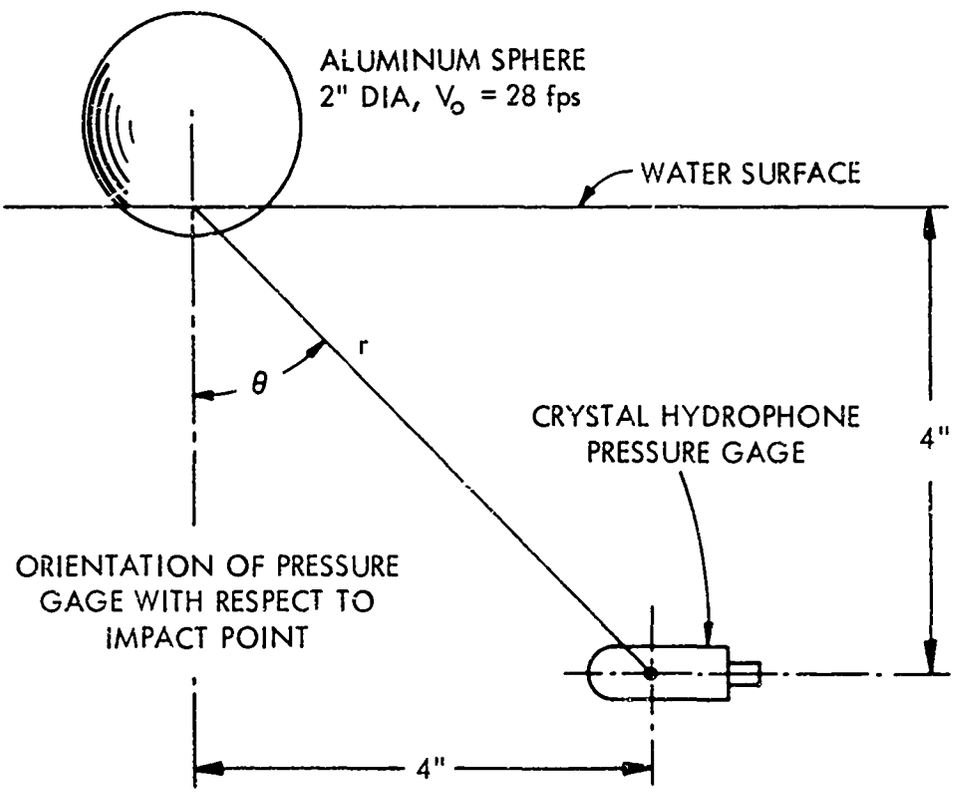

FIG. 1 A TYPICAL IMPACT PRESSURE RECORDING

The oscilloscope sweep was triggered by the use of another pressure gage placed above and to one side of the pressure pickup gage.

At the moment the sphere touches the water surface, the pressure gage gives out an impulse signal rising to a finite value in some time less than five microseconds. Approximately 30 microseconds later the signal lowers to a constant value of about one-third its former peak, remaining there for a time greater than 400 microseconds.

The peak pressure recorded by this gage in the above case is 0.356 psi (above its original static pressure). The gage is located 5.66 inches away from the impact point and 45 degrees from the line of entry. The theoretical impact pressure, ρcV, on the nose of the sphere is 1,815 psi. The large difference cannot be explained by any correction of the radius and direction angle to the gage. It is therefore assumed, and very reasonably so, that the pressure gage "undershoots" impulsive pressure rises imposed upon itself. The "natural frequency" of the gage and the recording system is very high since the output rises to a peak value in less than 5 microseconds, but an infinite natural frequency would be required to read the 1,815 psi value.

The shape of the pressure pulse just discussed will be analyzed in the following sections.

Dipole Theory. The dipole theory (Appendix A) enables one to calculate the pressure generated in the surrounding fluid by a vibrating solid sphere. For this first approximation, the time history of the force acting on the sphere need only be known. This first approximation is based on the result that the motion of the sphere (and hence its velocity and acceleration) may be assumed to be composed of an infinite sum of cosine terms, varying both in frequency and amplitude.

In this case the resulting pressure generated at a point in the fluid due to the motion of a sphere passing into the fluid while under the influence of a time varying force F(t) is

$$p = \frac{\cos\theta}{8\pi}\left[\frac{\frac{r}{c}}{r^2}F(t-c) + \frac{\frac{r}{c}}{rc}\right] \qquad (1)$$

where p = pressure at some point in the fluid

θ = the directional angle to the point

r = distance to the point

c = speed of sound in the fluid

t = time

In the above equation the term that is proportional to $1/r$ is generally called the far-field term while the term that is proportional to $1/r^2$ is called the near-field term.

The force F(t) may be read directly from the pressure equation if the voltage from the pressure transducer is fed into an electronic low-pass filter (Appendix A). The equation of the filter is similar to the pressure equation. The RC time constant of the filter must equal the ratio r/c; i.e., the ratio of the radius to the pressure pickup point over the speed of sound in the fluid. When the output of the low-pass filter is multiplied by $8\pi r^2/\cos\theta$, the resulting number will be the axial force acting on the sphere.

The results of the preceding equations will be compared later to theoretical and experimental results of the author and other experimental and theoretical investigators.

Momentum Equation. A theoretical equation for the acceleration produced on a sphere at water-entry impact has been derived in Appendix B. The theory closely parallels von Karman's investigation into the stress analysis of seaplane floats during landing. The acceleration is found to be a function of the virtual mass of the sphere which changes as a function of the depth of submergence of the sphere below the water surface.

The final equation for the water-entry acceleration on a 2-inch-diameter aluminum sphere is:

$$\frac{d^2y}{dt^2} = \frac{-V_o\ (0.345)x(1-y)\ dy/dt}{\left[1 + 0.115\ x^3\right]^2} \qquad (2)$$

where y = the penetration of the sphere below the water surface

V_o = the initial water-entry velocity of the sphere

x = the radius of the circle which is the intersection of the sphere and the plane water surface

t = time; all lengths are in inches and time is in seconds.

The above equation for the acceleration of the sphere was solved in incremental steps of y in ten thousandths of an inch. The velocity was corrected at each increment since the sphere suffered a continual attrition of speed as it passed through the water surface.

After the acceleration of the sphere was determined, the impact drag coefficient was calculated by use of the following relationship:

$$C_D = \frac{-2m\ddot{y}}{\rho A V_o^2} \tag{3}$$

where C_D = impact drag coefficient

m = mass of the sphere

ρ = density of the water

A = maximum cross-sectional area of the sphere

V_o = initial entrance velocity of the sphere.

The average impact pressure across the wetted area of the sphere was then determined as the ratio of the force acting on the sphere to the intersected cross-sectional area; i.e., $m\ddot{y}/\pi x^2$.

The above equations will be compared in a later section to the results of other experimental and theoretical investigators.

Shiffman and Spencer Theory. More than 15 years ago Drs. Shiffman and Spencer, reference (11), of the Applied Mathematics Group at New York University determined mathematically the force acting on a body with a spherical nose during its water-entry impact phase.

The solution approximated the sphere by an expanding lens and took into account the disturbance of the surface of the water. The disturbance of the water surface led to two types of corrections for the water-impact force on the sphere. The first correction took into account the upward rise of the surface of the water as it wets a larger portion of the entering sphere, thereby increasing the resistance of the water to the entering body. Secondly, the rising surface relaxes somewhat the restraint imposed on the body, thereby causing a decrease in the impact force. These two corrections partly counterbalance each other. The disturbance of the water surface was analyzed by using a combination of theory and results derived by experiment.

The theoretical results of Shiffman and Spencer will be compared in a later section to the results of other theoretical and experimental investigators.

Mosteller Experiments. Less than ten years ago, Mosteller, reference (12), at the Naval Ordnance Test Station, China Lake, determined experimentally the water-entry force on a spherical nosed model striking the water vertically.

He launched 2-inch-diameter spherical nosed models at low velocities (25-75 fps) and various angles (15-90 degrees) into water. The models were instrumentated with barium-titanate crystal accelerometers, the signal-out coaxial cable hanging freely to a fixed point in the launching tank.

It should be pointed out that the recorded acceleration at water entry is a function of (1) the water-entry forcing function, (2) missile-body response, (3) accelerometer response, and (4) the response of the recording system. Mosteller, however, was able to discriminate between forcing function and body response by the use of low-pass filters on the output of the crystal accelerometer. These filters allowed the passage of the low-frequency components of the water-entry forcing function and attenuated the relatively high-frequency components of the body response to a negligible value.

The most accurate drag coefficient curves given by Mosteller are the ones for which the data were taken at an entrance velocity of 25 fps. This is a result of the low-frequency cutoff of the filter used and, hence, its inability to follow the rise of the input signal. The effect of the missile-body response is also less at these lower entrance velocities.

The experimental results of Mosteller will be compared in a later section to the results of other theoretical and experimental investigators.

Open Cavity Flow, Half-Body Theory

The shape of the cavity produced by the entrance of a sphere into water may be approximated by the shape of a half-body in a uniform flow. (Appendix C)

The shape of the water-entry cavity produced by a 2-inch-diameter sphere may be approximated on a polar coordinate graph by:

$$r = \text{secant } \frac{\theta}{2} \tag{4}$$

where r = radial distance, in inches, to the point on the half-body

θ = directional angle, in radians, to the point.

The shape of the cavity as produced by the vertical entry of a 2-inch-diameter model into water will be compared later to the shape of the theoretical half-body.

Pressure Around the Open Cavity. The pressure at any point in the fluid due to the motion of the cavity through the fluid is predicted by the half-body theory (Appendix C) for a 2-inch-diameter sphere as;

$$\frac{\Delta p}{\frac{1}{2}\rho U^2} = 2\, r^{-2} \cos\theta - r^{-4} \tag{5}$$

where Δp = rise in pressure at a point over the pressure at infinity

r = ratio of the radial distance to the radius of the sphere

θ = directional angle, in radians, to the point

ρ = density of the fluid

U = velocity of the sphere.

In the above equation the instantaneous velocity of the sphere is used for U instead of holding the velocity of the sphere, U, constant. This adjusted velocity correction is applied to the motion of the sphere by assuming that the cavity drag coefficient of the sphere is equal to 0.30 (as measured by standard water-tunnel techniques). By this method, the steady state nature of the potential flow solution to the half-body problem is transposed to a pseudo-steady state problem, thus allowing a correction to the ever changing velocity of the sphere. This is a reasonable assumption to make for an approximate solution to the pressure distribution around the half-body since the change of velocity of the sphere, with respect to time or distance, is not violent.

The pressure as predicted by the half-body pressure equation will be compared in a later section to the pressure as predicted by the velocity-corrected half-body solution and also to actual pressure measurements made at a point in the water.

Pressure in the Cavity. As the sphere passes through the water surface and generates an open cavity behind it, one would not expect that the pressure in the cavity will deviate too much from the atmospheric pressure or local hydrostatic value on the wall of the cavity, reference (5).

Also, the pressure across the cavity wall would not be expected to be discontinuous, although the space derivative of this pressure at the cavity wall may be discontinuous.

Many difficulties arise when one attempts to measure the pressure in a cavity behind a moving body, reference (5). If the pressure measuring instrument is mounted in the missile, it must withstand the impact forces and deceleration applied to it while trying to monitor the minute pressure changes in the cavity. The pressure instrument must not be sensitive to acceleration and a means must be provided to record the pressure signal.

Reference 7 describes an attempt made approximately fifteen years ago to measure the cavity made by a water-entry missile. The pressure transducer used was of a rather bulky nature and the velocity of the model was low. An examination of the motion picture films revealed that the pressure transducer was not in the cavity, but rather that the cavity flowed around the gate. The pressure gate refused to penetrate the cavity wall, probably

due to the low radial velocity of the cavity wall and the surface tension of the water.

The pressure gages used in the present investigation are of such a small size and configuration so as to allow penetration of the cavity wall by the gage. The pressures have been taken at a point in the water as the water-entry cavity was allowed to envelope the pressure gage.

The pressure in the cavity has been approximated by use of the pressure equation as derived for the half-body flow theory (Appendix C). A velocity correction has also been applied to this theory.

The comparison of these three results will be made in a later section.

Bubble Oscillation at Cavity Collapse

As the water-entry cavity collapses, the closure seals the atmosphere from the lower portion of the cavity and the model. This lower portion of the cavity will then pulsate in a volume mode as it moves along with the missile.

The volume attached to the missile has been approximated as a bubble and the frequency of oscillations of the bubble has been derived analytically in Appendix D.

High-speed motion pictures allow a visual observation of the pseudo-steady cavity (bubble) trailing the sphere. The dimensions of the cavity may be made from the film to determine its theoretical frequency of oscillation.

A comparison of the experimentally observed oscillation of the cavity bubble will be made, in a later section, with those predicted by the theoretical equation of the bubble oscillation.

COMPARISON OF EXPERIMENTAL AND THEORETICAL RESULTS

Impact Phase

Results of Dipole Theory. In order to test the validity of the dipole theory of water impact of a sphere entering water vertically (Appendix A), experimental tests were

performed using a pressure gage and an operational filter. Figure 2 is a typical example of one of these tests.

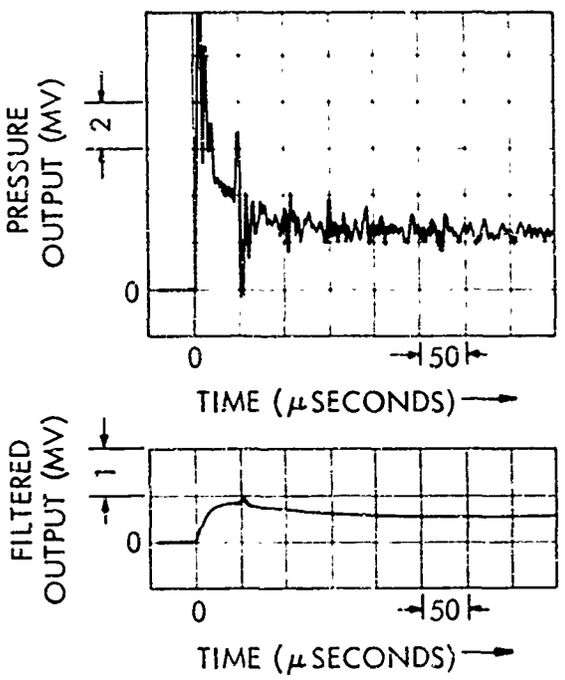

TEST PARAMETERS

SPHERE, ALUMINUM, 2 INCH DIAMETER.
WATER ENTRANCE VELOCITY, 29 fps.
PRESSURE GAGE, 14 INCHES BELOW WATER SURFACE AND 6 INCHES FROM TRAJECTORY OF SPHERE.
SENSITIVITY OF PRESSURE GAGE NO. 18, 6.85 psi/V
TIME CONSTANT OF RC FILTER, 260 μ SECONDS.

FIG. 2 PRESSURE TAKEN AT A POINT IN THE FLUID AND THE RESULTING OUTPUT OF THE OPERATIONAL FILTER

In this test a 2-inch-diameter aluminum sphere was dropped from a height of approximately 13 feet above the water surface. A 5-foot section of 2-1/4-inch I.D. glass tubing was used as an alignment for the dropped sphere. The pickup pressure gage was located approximately 14 inches below the water surface and 6 inches from the straight line trajectory of the sphere.

The first picture of figure 2 is a trace on the oscilloscope face as recorded by the pressure gage. The sensitivity of the gage used was 6.85 volts/psi. The sweeping rate of the scope was 50 μs/cm (50 microseconds per large division). The vertical amplifier sensitivity of the scope was 2 mv/cm (2 millivolts per large division); hence, 0.0137 psi/cm on the vertical scale. This is a typical pressure trace as recorded by a pressure gage placed beneath the water surface (i.e., similar to figure 1).

The second picture of figure 2 is a trace of the output of the operational filter, fed by the pressure gage just described above. The sweep rate again is 50 μs/cm but the vertical sensitivity is now 1 mv/cm. The scopes were triggered by a second pressure gage placed above and to one side of the pickup pressure gage.

The time constant of the operational filter was made equal to the distance between the impact point and the pressure gage divided by the speed of sound in the water. Thus,

$$R_o C_o = \frac{r}{c} = \frac{15 \text{ inches}}{4800 \text{ ft./sec.}} \cdot \frac{\text{ft.}}{12 \text{ inches}} = 260 \ \mu s \qquad (6)$$

Now the dipole theory says that we may multiply the output of the operational filter by $8\pi r^2/\cos\theta$ to obtain the force on the sphere. There is, of course, a time lag (phase factor) of r/c, the time required for the pulse to reach the pickup gage. From the lower picture of figure 2, the peak force felt by the sphere on water impact is then

$$F = \frac{8\pi r^2}{\cos\theta} p = \frac{8\pi (15.3 \text{ in.})^2}{0.923} \times \frac{6.85 \text{ psi}}{\text{volt}} \times \frac{0.002 \text{ volt}}{\text{cm}} \times 0.8 \text{ cm} \qquad (7)$$

or F = 70 pounds.

The peak impact drag coefficient for this force may then be calculated as:

$$F = \tfrac{1}{2}\rho\, C_D\, A\, V^2$$

$$70 \text{ lbs.} = \tfrac{1}{2}\left(62.4 \frac{\text{lb.}}{\text{ft.}^3}\right)\left(\frac{\text{sec.}^2}{32.2 \text{ ft.}}\right) C_D \pi \left(\frac{\text{ft.}}{12}\right)^2 \left(\frac{29 \text{ ft.}}{\text{sec.}}\right)^2$$

$$\text{or } C_D = 3.8 \qquad (8)$$

and the time to reach this peak is approximately 50 μs.

Sphere Vibrations. The high-frequency vibrations of the constant pressure trace shown in figure 2 indicate interesting phenomena. At first this occurrence was attributed to the ringing of the pressure gage; i.e., excitation of the natural frequency of the crystal pressure gage. The period of these vibrations is of the order of magnitude of 15 μs. The period of the natural frequency of the crystal is certainly much less than this since the rise time of the beginning of the trace is approximately five μs or less. The vibrations were then thought to be due to the sphere. Probably the most important mode of vibration excited in a rigid solid sphere falling vertically and striking the water surface is the spheroidal one. In this mode the sphere is distorted into an ellipsoid of revolution, and the frequency of this mode of vibration, reference 14, is given by

$f = \dfrac{0.3C_s}{a(1+\sigma)^{\frac{1}{2}}}$ where σ is Poisson's ratio for the sphere, a is the radius of the sphere, and C_s is the velocity of sound in the sphere. For the 2-inch-diameter aluminum sphere, the frequency and period of oscillation are given as:

$$f = 0.3\left(16{,}740 \frac{\text{ft.}}{\text{sec.}}\right) \frac{12 \text{ in./ft.}}{(1 \text{ in.})\ (1 + 0.332)^{\frac{1}{2}}} \qquad (9)$$

$$f = 52{,}300 \text{ cps}$$

and T = 19 μs; hence, it is concluded that the very high-frequency vibrations superimposed on the water impact pressure trace are due to the spheroidal vibrations of the aluminum sphere.

Momentum Equation Results. The results of the momentum equation previously described have been calculated as

outlined in Appendix B. The results of these equations have been plotted in figures 3, 4, 5, and 6. Figure 3 is a plot of the acceleration acting on the sphere ($-d^2y/dt^2$) versus time and the fraction of the radius that is submerged in the water. The impact is the result of the 2-inch-diameter aluminum sphere striking the water surface vertically with a velocity of 28 feet per second. The peak acceleration acting on the sphere is 17,500 in./sec.^{2} and occurs at 710 μs. This time of peak force occurs when the sphere has submerged approximately 25 percent of its radius below the water surface.

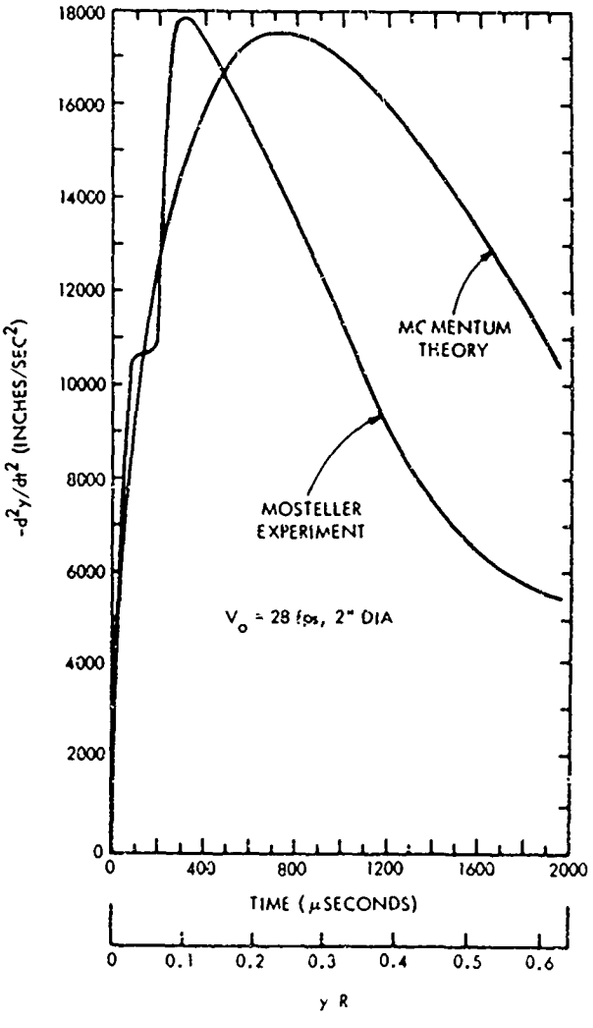

FIG. 3 WATER-ENTRY ACCELERATION OF A SPHERE VERSUS TIME (MOMENTUM THEORY AND MOSTELLER EXPERIMENT)

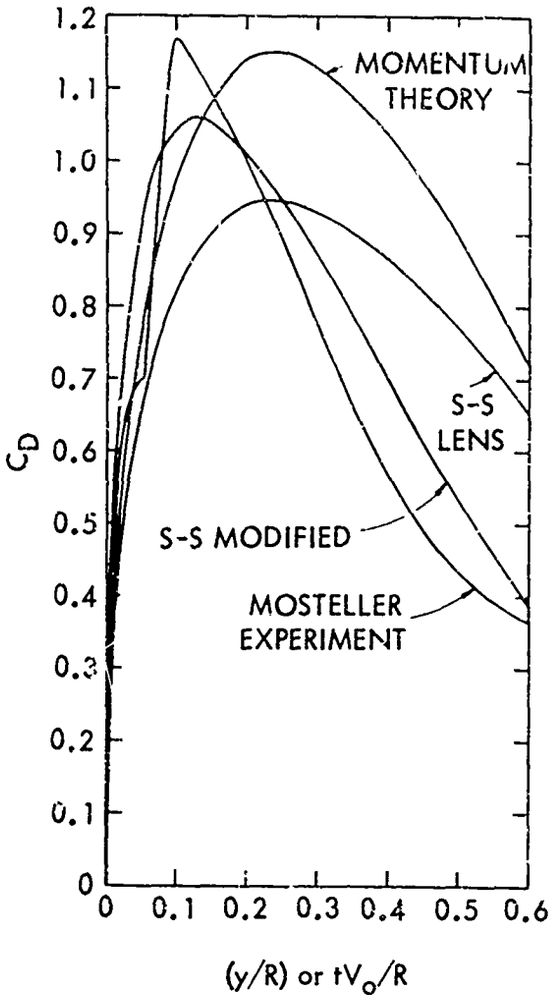

FIG. 4 DRAG COEFFICIENT FOR SPHERICAL-NOSE WATER ENTRY (SHIFFMAN-SPENCER LENS AND MODIFIED, MOMENTUM THEORY, AND MOSTELLER EXPERIMENT)

Figure 4 contains a plot of the drag coefficient of the sphere versus the fraction of the radius submerged below the water surface for the momentum equation theory. This is essentially the same curve as plotted in figure 3 since the drag coefficient is

$$C_D = \frac{-2m\ddot{y}}{\rho A V_o^2} \qquad (10)$$

The peak impact drag coefficient for the sphere is C_D (peak) = 1.15 and occurs

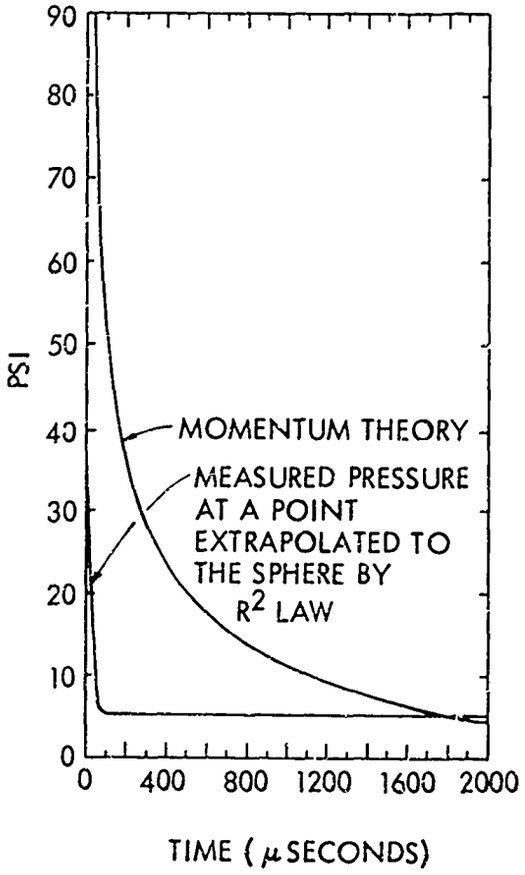

FIG. 5 AVERAGE PRESSURE ACROSS WETTED AREA OF SPHERE VERSUS TIME (MOMENTUM THEORY AND CORRECTED MEASURED PRESSURE)

at the same time just described above; i.e., when the sphere has submerged approximately 25 percent of its radius below the water surface.

Figure 5 contains a plot of the average pressure across the nose of the sphere versus time, as predicted by the momentum equation theory. The 2-inch-diameter aluminum sphere is striking the water surface with a velocity of 28 fps, as before. At time t = 0, the momentum theory predicts an infinite pressure across the face of the sphere. This occurs since the initial contact between the sphere and the water surface is essentially the same as the impact of a flat plate striking a flat water surface, both surfaces being initially parallel. An infinite pressure, of course, cannot occur when the sphere strikes the water surface due to the finite value of the compressibility of the water. Von Karman predicts an impact pressure, in this case, of a value equal to ρcV. For the sphere striking the water surface with a velocity of 28 feet per second, the effect of the compressibility on the impact pressure on the nose of the sphere is

$$\rho cV = \left(62.4 \frac{lb}{ft^3}\right)\left(32.2 \frac{sec^2}{ft}\right)\left(4800 \frac{ft}{sec}\right)\left(28 \frac{ft}{sec}\right)\left(\frac{ft^2}{144\ in^2}\right)$$

$$= 1810 \text{ psi} \qquad (11)$$

This value is approximately 18 times the maximum pressure shown on the graph. Since the momentum theory predicts a very sharp decrease from infinity in the average pressure across the face of the sphere, Von Karman's value of the impact pressure, ρcV, is a plausible value.

Figure 6 is an <u>extrapolation</u> of the average pressure (momentum equation across the face of an impacting sphere to a point that is 1 inch below the water surface and 2 inches from the line of impact). The extrapolation was assumed to be able to be performed in the following manner. The pressure at a point in the fluid was assumed to vary according (see figure 7) to the law

$$p(r, \theta) = p_o \cos \theta \left(\frac{r_o}{r}\right)^2 \qquad (12)$$

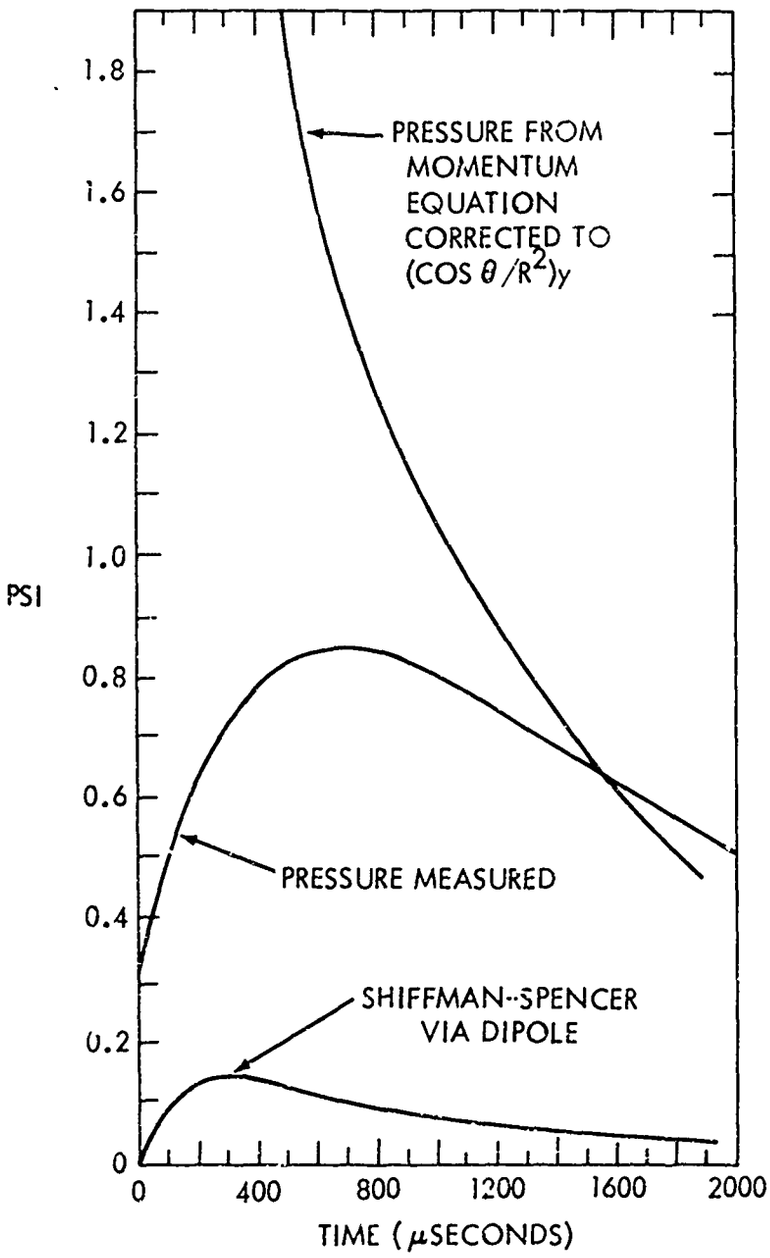

FIG. 6 IMPACT PRESSURE AT A POINT IN THE FLUID (CORRECTED MOMENTUM EQUATION, SHIFFMAN-SPENCER VIA DIPOLE THEORY, AND MEASURED PRESSURE)

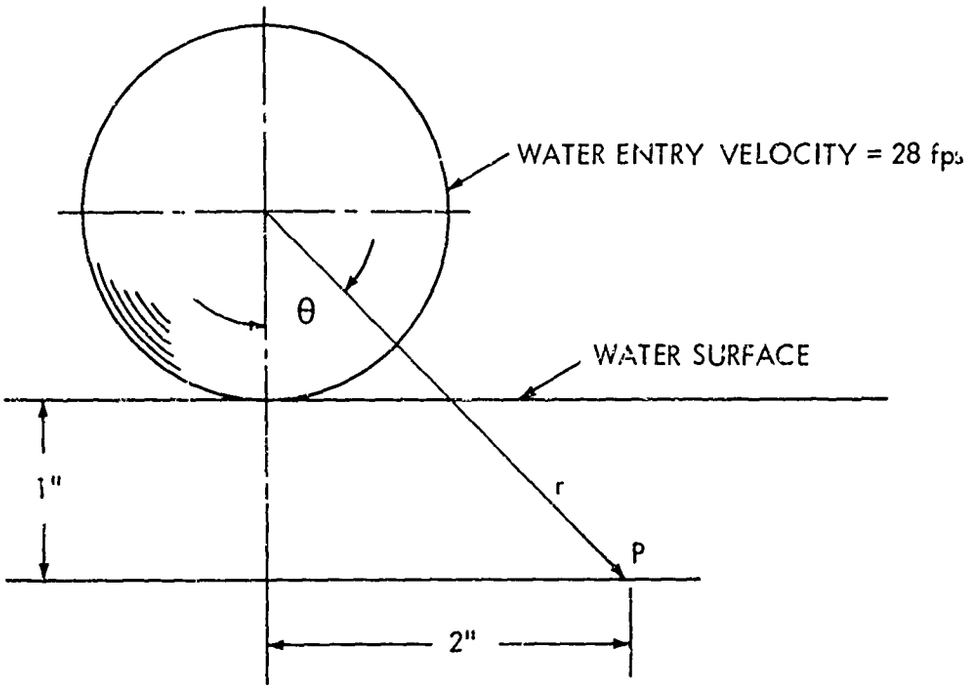

FIG. 7 CORRECTION APPLIED TO MOMENTUM EQUATION PRESSURE

This says that the pressure at a point in the fluid will decrease as the product of $1/r^2$ and the cosine of the direction angle. The value of r_o for the 2-inch sphere is 1 inch; hence,

$$p(r, \theta) = p_o \frac{\cos \theta}{r^2} .$$

The values of r and θ were calculated at various increments of the depth of submergence of the sphere below the water surface. The impact pressure as described by the momentum equation was then multiplied by the ratio $\cos \theta/r^2$ at the appropriate points for the depth of submergence of the sphere. The results of this equation are plotted in figure 6, the variables being pressure and time. The shape of the curve has the same general appearance as the shape of the results of the pressure across the face of the sphere as calculated by the momentum equation.

Shiffman and Spencer Theory. The results of the drag coefficient for the vertical water entry of a sphere as determined by Shiffman and Spencer, reference (11), are plotted on figure 4. The modified lens theory of Shiffman and Spencer takes into account the rise of the water surface around the sides of the sphere. The modified lens theory for the drag coefficient of the sphere peaks at a higher value and sooner than their first approximate theory for the flow about an expanding lens. The modified lens theory results in a peak impact drag coefficient of 1.06 occurring at a depth of submergence of 0.125 times the radius. This compares favorably with the results of the momentum equation plotted on the same graph.

Figure 6 contains a plot of the pressure resulting at a point as calculated by the dipole theory using the values of the drag coefficient of the modified Shiffman and Spencer theory. The F and $\dot{F}$ terms of the force on the sphere in the dipole theory were determined from the drag coefficient curve of Shiffman and Spencer. The analysis was carried out for the point that was 1 inch below the water surface and 2 inches to one side of the sphere's trajectory. The results of the analysis are compared, on the same graph, to the actual pressure measured at the point and the extrapolated pressure as predicted by the momentum equation. The agreement among the pressures resulting from these three methods is not too good. The extrapolated momentum equation pressure is generally much larger than the actual pressure measured while the Shiffman and Spencer-Dipole theory is generally smaller.

Mosteller Experimental Results. The results of the impact drag coefficient of a sphere as determined experimentally by Mosteller are presented in figures 3 and 4. The acceleration of the sphere as found by Mosteller is compared to the acceleration as predicted by the momentum equation (figure 3). The agreement between these two is very good. Mosteller found a peak impact drag coefficient, for the sphere, of 1.17 occurring at a depth of submergence of the radius of 0.10. The two theories for the impact drag coefficient of Shiffman and Spencer are plotted on figure 4 along with the results of Mosteller and the momentum equation. Agreement among all of the results is very good.

Cavity Flow Phase

After the sphere strikes the water surface, a cavity is formed behind the sphere. Figure 8 shows the sequence of events following the impact phase of the sphere. It is a

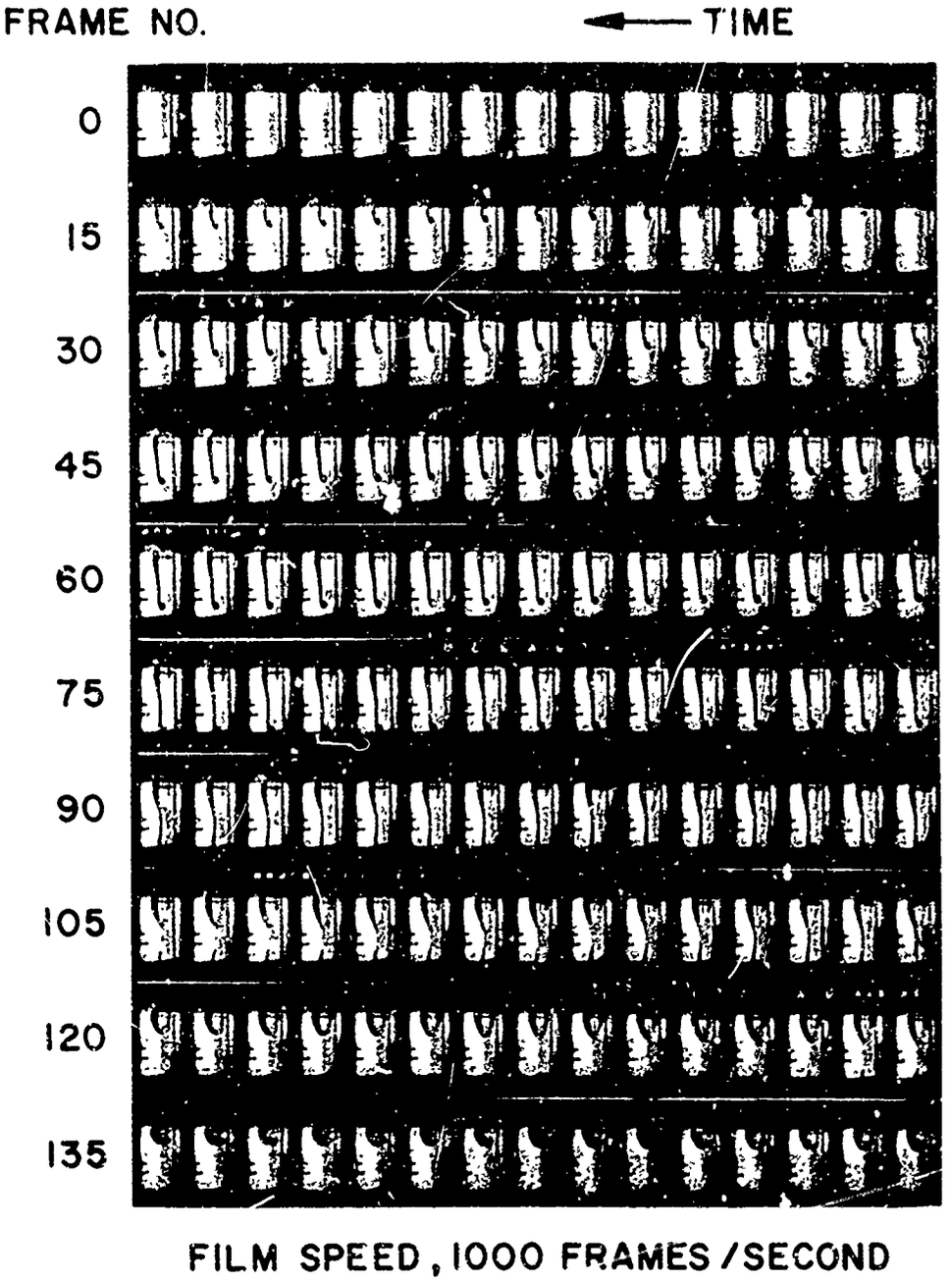

FIG. 8 WATER-ENTRY CAVITY PRODUCED BY A SPHERE
2-INCH-DIAMETER, ALUMINUM, 28 FT/SEC

contact print of high-speed 16-mm film taken during water entry of a 2-inch-diameter aluminum sphere striking the water surface at 28 feet per second. The film speed is approximately 1000 frames per second.

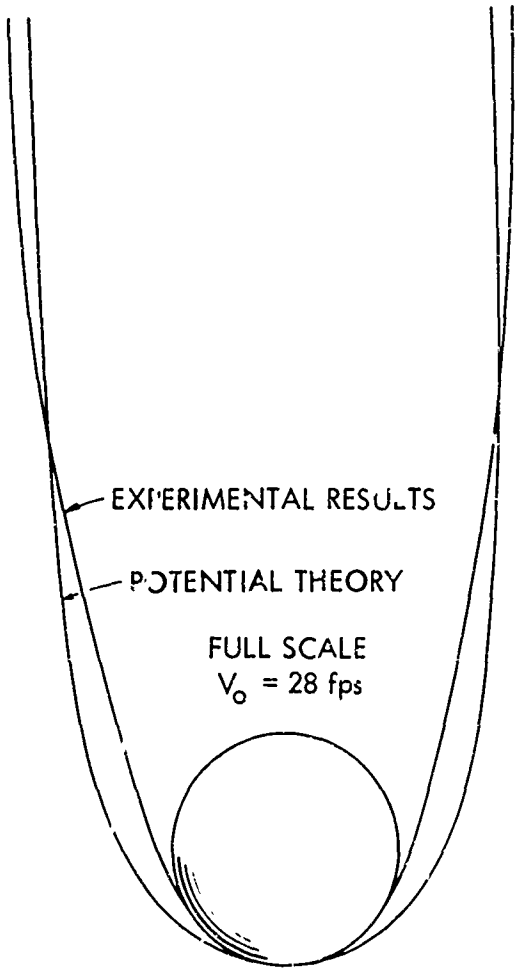

FIG. 9 COMPARISON OF AN ACTUAL CAVITY SHAPE WITH POTENTIAL THEORY SHAPE

One frame of this film (approximately frame No. 40) was projected onto a sheet of paper such that the nose of the cavity would coincide with a previously drawn 2-inch-diameter circle. The shape of the cavity as predicted by potential flow theory of the half-body (Appendix C) was then plotted on the same paper. These results are shown in figure 9. The nose of the actual cavity is more pointed than that predicted by the half-body approximation, but the comparison is more favorable on the after-body section.

Open Cavity Pressure Results. Figure 10 is a composite of pictures taken of the pressure trace of a gage placed 12 inches below the water surface and 6 inches to one side of the trajectory of the sphere. The 2-inch-diameter aluminum sphere is striking the water surface at 28 feet per second. The vertical scale of each of the pictures is the same, 0.0307 psi/cm, but the time scale of each picture is different. The first picture describes the impact phase, as previously discussed. The following pictures in figure 10 describe the approach of the sphere to the pressure gage.

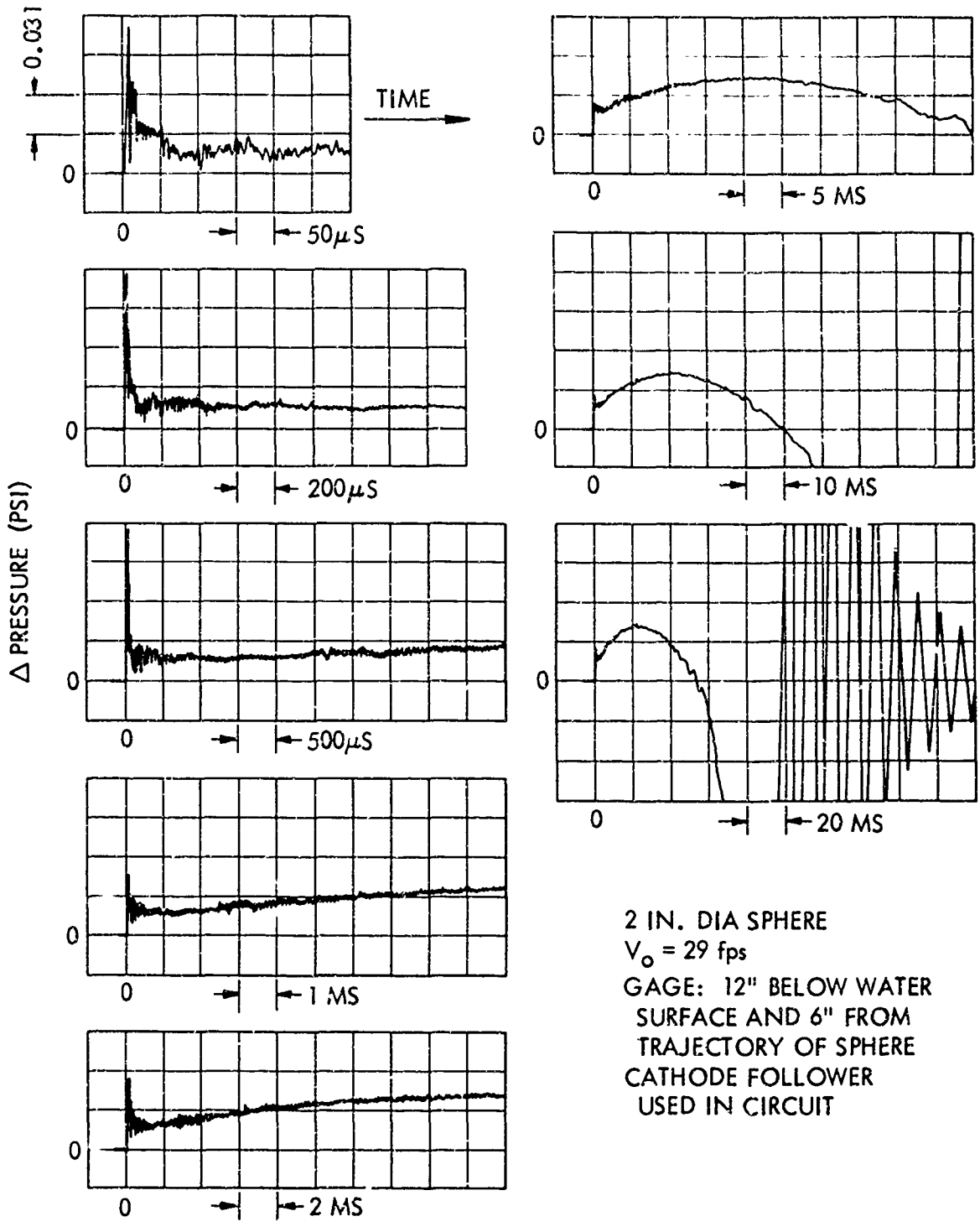

FIG. 10 COMPLETE PRESSURE RECORDS OF THE WATER ENTRY OF A SPHERE

A better view of the pressure trace just described may be had in figure 11. This has been composed of four pictures from figure 10 such that one continuous pressure trace results. The vertical pressure scale is constant over all of the trace; the time scale changes in each of the four divisions of the trace. The position of the sphere at various times is indicated above the pressure trace.

The rise in pressure as the sphere approaches the gage (figures 10 and 11) has been plotted on figure 12 and is compared to the pressure predicted by the half-body theory (Appendix C). When the velocity correction is applied to the pressure predicted by the half-body theory, agreement is obtained with the actual pressure measured (within 10 percent). This analogy has not been carried on past the point when the sphere is opposite the pressure gage. At this time figure 8 shows that the cavity is starting to close; hence, it does not maintain the shape as predicted by the half-body theory and the resulting pressures would not be expected to agree.

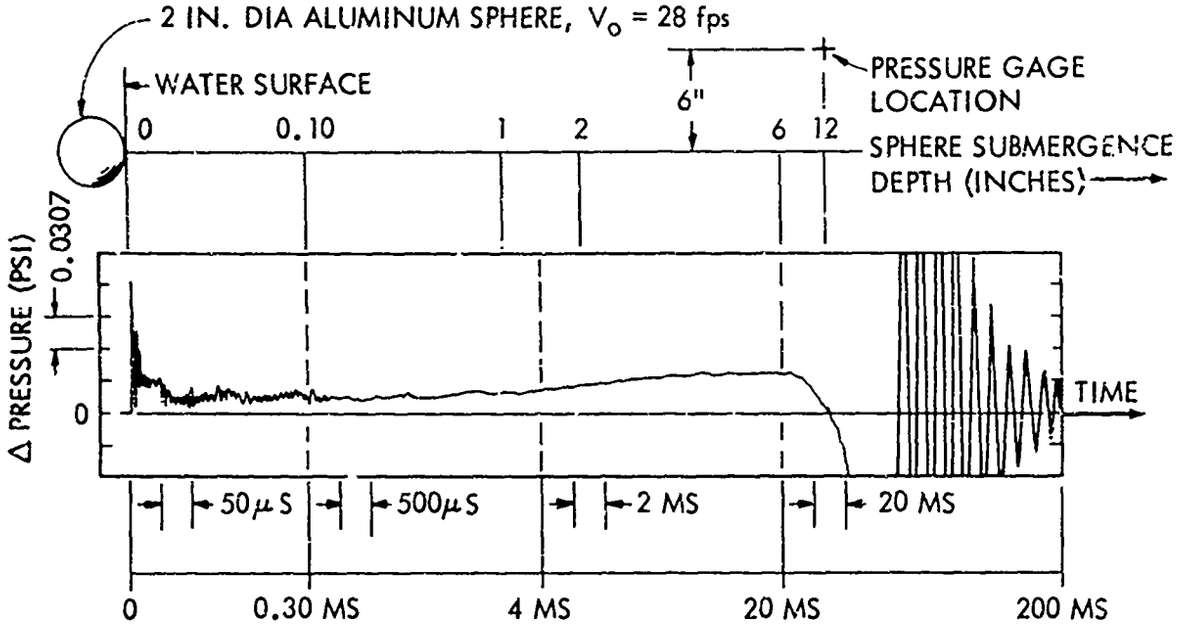

FIG. 11 COMPOSITE TRACE OF THE PRESSURE RECORD OBTAINED FOR THE WATER ENTRY OF A SPHERE

This closing of the cavity results in a higher negative pressure than the half-body theory would predict and is not included on the graph since the analogy breaks down.

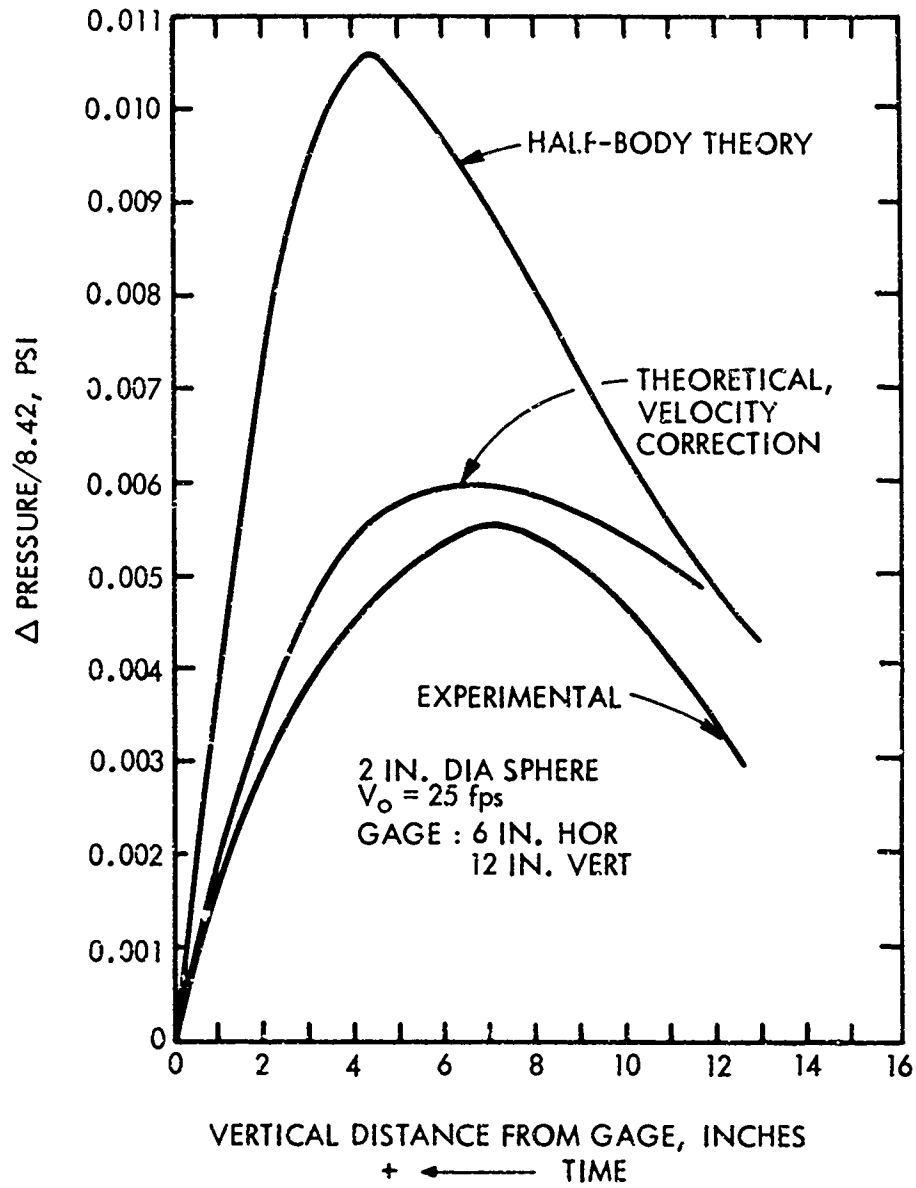

FIG. 12 PRESSURE IN THE FLUID DUE TO CAVITY FORMATION

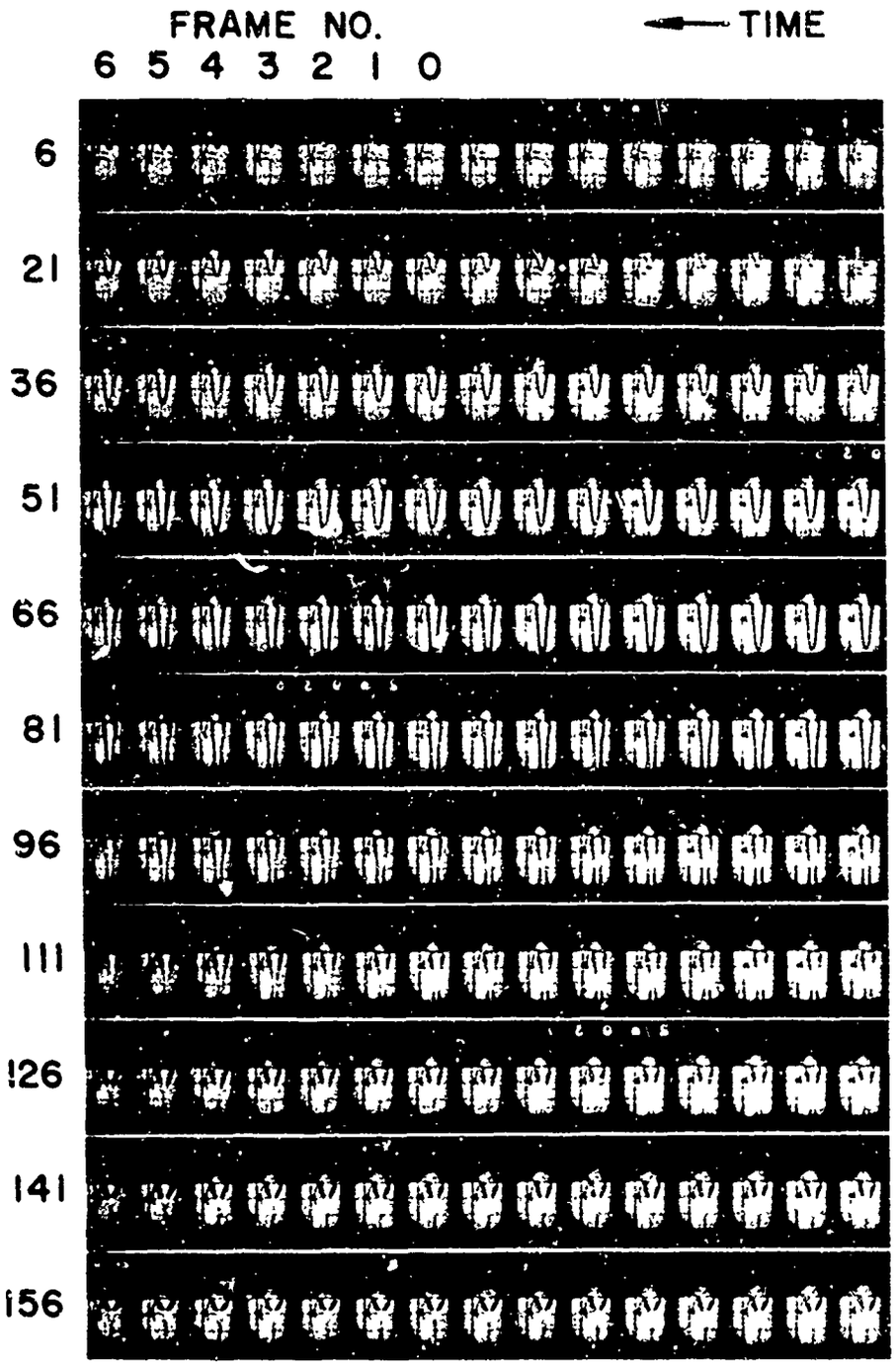

FIG. 13 MOTION OF A WATER-ENTRY CAVITY PAST A PRESSURE GAGE

Measured Pressure in the Cavity. In order to place a pressure gage in a water-entry cavity, the cavity had to be allowed to expand around the gage. The pressure gage in figure 8 (lower prong, left-hand side) was never in the water-entry cavity at any time. To get the pressure gage into the cavity a test was performed whereby the gage was placed 5 inches below the water surface, and the acoustic center of the pressure gage was placed 2 inches from the straight line trajectory of the sphere. Figure 13 is a contact print showing the pressure gage in the cavity. The lower prong in the pictures is the pressure gage (in the plane of the pictures) while the upper prong is the trigger gage (rotated away from the pressure gage). The pressure gage was determined to be in the cavity for several reasons. The pressure gage was positioned as close as possible to the trajectory of the sphere. In some instances the sphere actually brushed the tip of the gage, as determined by off-scale spikes of the pressure trace. Frame No. 51 (for instance) shows a clearer image of the pressure gage than of the trigger gage. This is because the trigger gage is positioned just behind the cavity. Light from the trigger gage must travel through two walls of the cavity, thereby blurring the image. The background of the picture, which is 2-1/2 feet behind the cavity, does not photograph at all through the cavity. Frames 141 through 146 show the pressure gage coming out of the upper cavity after point closure. Surface tension between the water and the neoprene covering on the pressure gage results in a small meniscus as the cavity pulls away from the tip of the pressure gage.

The pressure trace from the gage of figure 13 is plotted on figure 14 along with the theoretical calculations of the half-body theory (Appendix C). The agreement between the two is very good both in time and magnitude.

Bubble Oscillation

Figure 15 is a lower view of the water-entry cavity and a continuation of figure 8. The cavity closure results in the high pressures recorded in figures 10 and 11. The low frequency of oscillation recorded at activity closure may be attributed to the transient nature of the formation of the closed bubble (closed cavity) around the sphere.

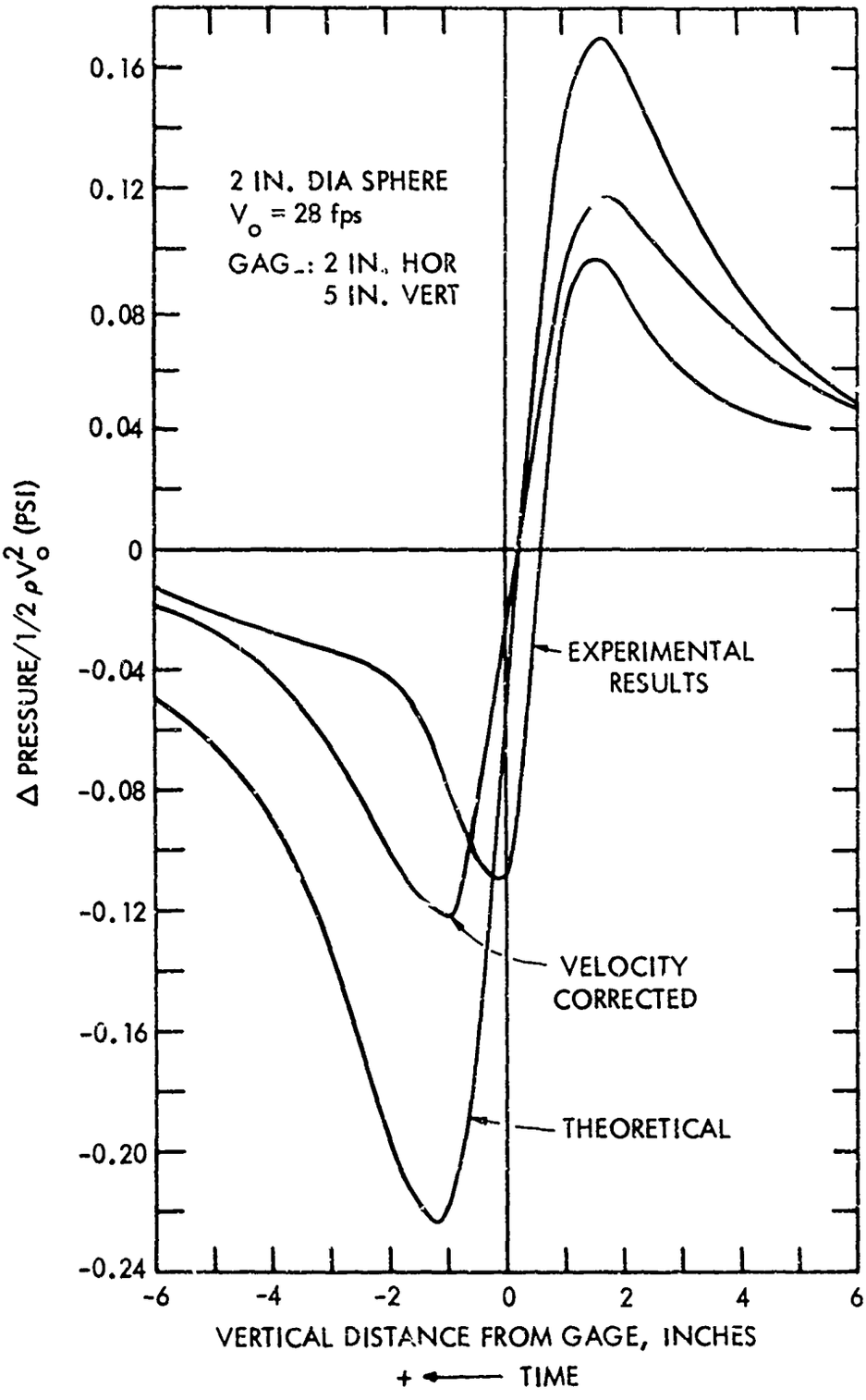

FIG. 14 PRESSURE IN THE WATER-ENTRY CAVITY

SPHERE, ALUMINUM, 2 INCH DIAMETER
V_o = 28 fps

FIG. 15 DEEP SEAL OF THE WATER-ENTRY CAVITY AND BUBBLE FORMATION

A spherical bubble of gas will oscillate according to the frequency equation (Appendix D):

$$T = 2\pi r_o \left[\frac{\rho}{3pk}\right]^{1/2} \tag{13}$$

where T = period of oscillation

r_o = mean radius of bubble

ρ = density of the surrounding fluid

k = ratio of specific heats of the gas in the bubble

p = pressure in the fluid surrounding the bubble

The bubble around the sphere is approximately three inches in diameter (figure 15). This bubble is approximately 18 inches below the surface of the water, where the surrounding pressure is 15.335 psia. The period of a spherical bubble of oscillation may then be given as the following, if air, k = 1.4, is assumed to be the gas in the bubble:

$$T = 2\pi(1.5 \text{ in.}) \left[\frac{0.03615 \text{ lb./in.}^3}{(3)\ (1.4)\ \left(15.335 \frac{\text{lb.}}{\text{in.}^2}\right)\ \left(386 \frac{\text{in.}}{\text{sec.}^2}\right)}\right]^{1/2}$$

$$T = 0.0113 \text{ sec.} \tag{14}$$

The period of oscillation of the bubble agrees very well with the period of oscillations found in figures 10 and 11. The volume change of the bubble cannot be detected in figure 15 since its motion is very small compared to the size of the bubble.

DISCUSSION OF RESULTS

The analysis of the water entry of missiles is a complicated problem. As shown in this report, the impact phase is the most difficult to analyze, both experimentally and theoretically, and rightly so, mainly due to its inherent transient nature.

The water-entry force on a sphere striking the water surface vertically has been approximated by the use of a momentum theory, not unlike von Karman's analysis of the landing impact on seaplane floats. The results of this theory compare well with the theoretical results of Shiffman and Spencer and the experimental results of Mosteller. Better results could probably be obtained if the effects of the free surface of the water were taken into account. Correlation, with theory, of the impact pressure measurements taken under water could not be obtained. The theoretical impact pressure, ρcV, of the sphere could not be detected with the crystal pressure gages.

The shape of the early water-entry cavity may be approximated by the potential theory of a source in a uniform flow. Good agreement is obtained between the shape of the cavity produced and that predicted by theory. Better correlation probably would result if a combination of sources and sinks was used instead of the single source. Pressures recorded in the water around the expanding water-entry cavity agree well with the pressures predicted by the potential theory for the cavity shape. This accuracy could be improved if a combination of sources and sinks was used.

Pressures measured in the cavity agreed well with those predicted by the potential theory for the cavity flow phase. There is some doubt whether or not this approximation is valid for pressures in the cavity since it is generally assumed that the cavity pressure is atmospheric when the cavity is open. If this were true, then the pressure records taken in the cavity would be hard to explain since a variation in pressure was recorded.

The frequency of vibration of the closed cavity after cavity collapse was closely correlated with the theory of a pulsating spherical bubble. Even though the shape of the cavity was not spherical, good agreement was obtained with the actual period of vibration measured.

The above analysis indicated that more effort must be brought to bear on the impact phase of the water entry of missiles, both experimentally and theoretically. It is suggested that:

1. The impact pressure distribution versus time be determined from large-scale water-entry drops of hemispheres. This should also be done with high-frequency crystal pressure gages and accelerometers.

2. The variation of the pressure in the fluid with distance and angle be determined considering the effect of the free surface.

REFERENCES

(1) Worthington, A. M., A Study of Splashes, Longman's Green, and Co., Inc., London, 1908

(2) Mallock, A., "Sounds Produced by Drops Falling on Water," Proc. Roy. Soc., London, A95, 1918

(3) Minnaert, M., "On the Musical Air-Bubbles and the Sounds of Running Water," Phil. Mag. 16, 235, 1933

(4) Milne-Thomson, L. M., Theoretical Hydrodynamics, MacMillan and Co. Limited, London, 1938

(5) Richardson, E. G., "Impact of a Solid on a Liquid Surface," Proc. Phys. Soc., London, 61, 352, 1948

(6) Richardson, E. G., "Sounds of Impact of a Solid on a Liquid Surface," Proc. Phys. Soc., London, B68, 1955

(7) May, A., "Vertical Entry of Missiles into Water," J. Appl. Phys. 23, 1362, 1952

(8) May, A., and Hoover, W. R., "A Study of the Water-Entry Cavity," NOLTR 63-264, 1964

(9) Lamb, H., The Dynamical Theory of Sound, Dover Publications, Inc., New York, New York, 1925

(10) von Karman, Th., "The Impact of Seaplane Floats During Landing," NACA TN 321, 1929

(11) Shiffman, M., and Spencer, D. C., "The Force of Impact on a Sphere Striking a Water Surface," AMP Report 42.2R, AMG-NYU No. 133, 1945

(12) Mosteller, G. G., "Axial Deceleration at Oblique Water Entry of 2-inch-Diameter Models with Hemisphere and Disk-Cylinder Noses," NAVORD Report 5424, 1957

(13) Stelson, T. E., "Acceleration of Bodies in Fluids--A Study of Virtual Mass," PhD Dissertation, Department of Civil Engineering, Carnegie Institute of Technology, 1952

(14) Franz, G. J., "Splashes as Sources of Sound in Liquids," J. Acoust. Soc. Am. 31, 1084, 1959

(15) Degarabedian, P., "Compressibility Effects during Water Entry," NAVORD Report 3523, 1955

APPENDIX A

DERIVATION OF THE DIPOLE THEORY

By means of a dipole theory it is possible to calculate the pressure generated in the surrounding fluid by a vibrating solid sphere. Lamb (reference (9)) states that "this is almost the only problem of the kind which can be completely solved," and "the results throw a good deal of light on other cases."

Let the velocity of the sphere be expressed in complex notation as

$$U = Ae^{int} \tag{A-1}$$

The velocity potential of a dipole Ce^{int} at the origin is

$$\Phi = \frac{-C}{4\pi} \frac{\partial}{\partial r} \left(\frac{e^{-ikr}}{r} \right) \cos\theta \quad k = n/c \tag{A-2}$$

and when the partial differentiation is performed

$$\Phi = \frac{C}{4\pi} \left(\frac{1 + ikr}{r^2} \right) e^{-ikr} \; e^{int} \; \cos\vartheta \tag{A-3}$$

Let us examine the case when $kr \ll 1$.

Then

$$r \ll \frac{1}{k} = \frac{c}{n} = \frac{\lambda f}{n} = \frac{\lambda}{2\pi} \tag{A-4}$$

and hence at points less than $\lambda/2\pi$, kr will be less than 1. When the radius a of the sphere is small compared with $\lambda/2\pi$, then in the immediate neighborhood of the sphere, the velocity potential can be reduced to

$$\Phi = \frac{C}{4\pi} \frac{e^{int}}{r^2} \cos\vartheta \tag{A-5}$$

The radial velocity of the fluid on the sphere is then

$$V_r\Big|_{r=a} = \frac{-\partial\phi}{\partial r}\Big|_{r=a} = \frac{C}{2\pi}\frac{e^{int}}{a^3}\cos\theta \qquad \text{(A-6)}$$

This must be equal to the velocity of the sphere at the same point, which is

$$U\cos\theta = Ae^{int}\cos\theta \qquad \text{(A-7)}$$

The constant is then found to be $C = 2\pi a^3 A$.

The complete solution for the velocity potential is then

$$\phi = \frac{a^3 A}{2}\left(\frac{1 + ikr}{r^2}\right)e^{-ikr}\ e^{int}\ \cos\theta \qquad \text{(A-8)}$$

The reaction on the sphere due to the fluid may be calculated by dividing the surface of the sphere into zones by planes perpendicular to the direction of motion of the sphere, Thus,

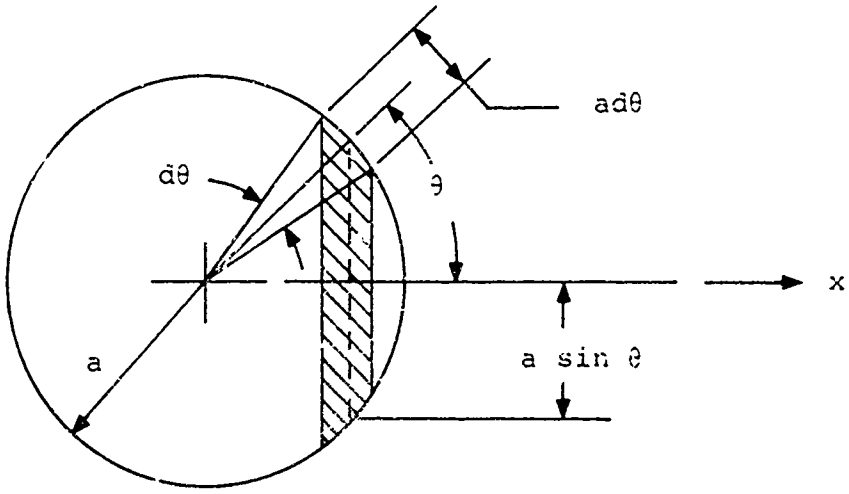

The increment of force in the x-direction on one of the zones is

$$dF_x = -p\pi(2a\sin\theta)a\,d\theta\cos\theta \qquad \text{(A-9)}$$

For any instant velocity U of the sphere, the velocity potential reduces to

$$\phi = \frac{Ua^3}{2r^2} \cos\theta \tag{A-10}$$

The pressure on the sphere is then found by

$$p\Big|_a = \rho \frac{\partial \phi}{\partial t}\Big|_a = \frac{1}{2} \rho\, a \frac{dU}{dt} \cos\theta$$

and $$F_x = -\int_0^{\pi} \frac{\rho a \dot{U} \cos\theta}{2} \pi\, 2a \sin\theta\, a\, d\theta \cos\theta$$

$$F_x = -\rho\, a^3\, \pi\, \dot{U} \int_0^{\pi} \sin\theta \cos^2\theta\, d\theta$$

$$F_x = -\rho\, a^3\, \pi\, \dot{U} \left| -\frac{\cos^3\theta}{3} \right|_{\theta = 0}^{\theta = \pi}$$

$$F_x = -\frac{2}{3} \rho\, a^3\, \pi\, \dot{U} \tag{A-11}$$

The force on the sphere is independent of its velocity and depends only on the acceleration of the sphere.

The equation of motion of the sphere can be written as:

$$M \frac{dU}{dt} = -\frac{2}{3} \rho\, a^3\, \pi\, \dot{U} + F(t) \tag{A-12}$$

where M = mass of sphere

U = velocity of sphere

ρ = density of fluid

a = radius of sphere

F(t) = extraneous forces on sphere

and then

$$\left(M + \frac{2}{3} \pi \rho\, a^3\right) \frac{dU}{dt} = F(t) \tag{A-13}$$

We originally let the velocity of the sphere be $U = Ae^{int}$. Let the extraneous force applied to the sphere be $F(t) = F_o e^{int}$. Substituting into the above equation for a sphere of the same density as the fluid,

$$\left(\frac{4}{3}\pi\rho a^3 + \frac{2}{3}\pi\rho a^3\right) Aine^{int} = F_o e^{int}$$

or
$$A = \frac{F_o}{2\pi a^3 \rho in} \tag{A-14}$$

When the expression for A is substituted back into the equation for the velocity potential, we have

$$\phi = \frac{F_o e^{int}}{4\pi\rho cik}\left(\frac{1 + ikr}{r^2}\right) e^{-ikr}\cos\theta \tag{A-15}$$

The pressure at any point can then be found from $p = \rho\dot{\phi}$,

$$p = \frac{\rho in F_o e^{int}}{4\pi\rho cin/c}\left(\frac{1 + ikr}{r^2}\right) e^{-ikr}\cos\theta$$

$$p = \frac{\cos\theta}{4\pi}\left[\frac{F_o e^{int}}{r^2} + \frac{in F_o e^{int}}{rc}\right] e^{-ikr}$$

$$p = \frac{\cos\theta}{4\pi}\left[\frac{F(t - r/c)}{r^2} + \frac{\dot{F}(t - r/c)}{rc}\right] \tag{A-16}$$

From the above equation one can find the pressure generated at a point in the fluid due to the motion of a sphere (of the same fluid) under a force $F(t) = F_o e^{int}$.

But since the fluid is only on <u>approximately</u> one side of the sphere, the pressure equation should be halved; hence,

$$p = \frac{\cos\theta}{8\pi}\left[\frac{F(t - r/c)}{r^2} + \frac{\dot{F}(t - r/c)}{rc}\right] \tag{A-17}$$

<u>Operational Filter</u>. The equation for the output of a low-pass electronic filter may be written as follows:

$$R_o C_o \frac{d(\theta/C_o)}{dt} + \theta/C_o = E(t) \tag{A-18}$$

If the sphere is of aluminum instead of the same fluid, say water, then the expression for p is found from the following:

$$p = \frac{\cos\theta}{8.68\pi}\left[\frac{F(t - r/c)}{r^2} + \frac{\dot{F}(t - r/c)}{rc}\right] \qquad \text{(A-19)}$$

This would be a more accurate indication of the pressure.

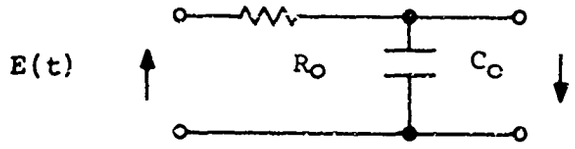

(A-20)

where E(t) = the input voltage

V_{out} = the output voltage

R_o = resistance of the circuit

C_o = capacitance of the circuit

q = charge

The voltage out across the capacitance of the filter circuit is

$$V_{out} = q/C_o \qquad \text{(A-21)}$$

The pressure equation from the following section may be written as follows:

$$\frac{r}{c}\dot{F}(t - r/c) + F(t - r/c) = \frac{8\pi r^2}{\cos\theta}\, p \qquad \text{(A-22)}$$

The pressure equation and the filter equation are quite similar. If the time constant (R_o C_o) of the filter circuit is made equal to the ratio r/c (the radius to the pressure pickup point over the speed of sound in the fluid), the output across the capacitor may be multiplied by $\frac{8\pi r^2}{\cos\theta}$ to give directly the axial force acting on the sphere.

APPENDIX B

DERIVATION OF THE MOMENTUM EQUATION

In connection with his investigation into the stress analysis of seaplane floats during landing, von Karman presented his famous approximation to the problem by use of the momentum equation and found that his theoretical results checked very well with experimental results. This has been applied to the water-entry problem of spheres in a similar manner.

Consider a sphere perpendicularly piercing a water surface, as follows:

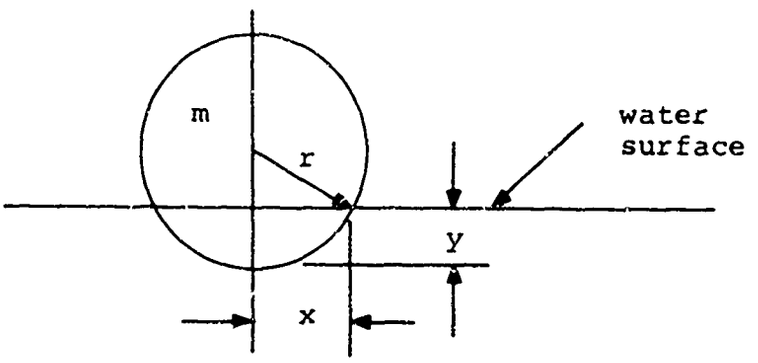

where m = the mass of the sphere

r = the radius of the sphere

y = depth of penetration of the sphere below the water surface

x = the radius of that circle which is the intersection of the undisturbed water surface and the sphere.

The total momentum equation for the system can be written as follows:

$$mV_o = mv + f(x)V \qquad \text{(B-1)}$$

where m = the mass of the sphere

V_o = the initial velocity of the sphere

V = the instantaneous velocity of the sphere

f(x) = some "added mass" of fluid that is moving with the velocity V of the sphere (varies with x).

The momentum equation can be written in the form:

$$V = \frac{V_o}{1 + f(x)/m} \tag{B-2}$$

The equation could now be solved, and the complete motion of the sphere could be determined, if the f(x) term were known.

As a first approximation to f(x), consider a thin flat circular plate moving in an infinite fluid. Added mass coefficients for this case are well known both theoretically and experimentally, reference (13). The presented cross-sectional area of the sphere to the water surface could be considered as a flat plate that changes dimensions with time (as shown in the diagram).

The added mass for a thin flat circular plate moving perpendicular to its surface is

$$(0.64)\rho\frac{4}{3}\pi x^3 \tag{B-3}$$

that is, the added mass is 64 percent of a sphere of fluid whose radius is equal to the radius of the plate. But in the case of the sphere entering water, fluid is moving on only one side of the imaginary plate; therefore, one-half of the apparent increase of mass for the plate is assumed. The term f(x) can be written as

$$\frac{0.64}{2}\ \rho\frac{4}{3}\pi x^3 \tag{B-4}$$

Solving the equation for V is now simple. We have that

$$V = \frac{dy}{dt} = \frac{V_o}{1 + \frac{f(x)}{m}} \tag{B-5}$$

and differentiating the expression for the velocity with respect to time, we have

$$\frac{d^2y}{dt^2} = -\frac{V_o}{m}\left[1 + \frac{f(x)}{m}\right]^{-2} \frac{df(x)}{dx}\frac{dx}{dt} \qquad \text{(B-6)}$$

which is the acceleration of the sphere.

From the geometry of the sphere entering the water surface, we have that

$$r^2 = x^2 + (r - y)^2$$

$$\text{or} \quad x^2 = 2ry - y^2 \qquad \text{(B-7)}$$

Differentiating the above expression with respect to time and solving for dx/dt, we find that

$$\frac{dx}{dt} = \frac{r - y}{x}\frac{dy}{dt} \qquad \text{(B-8)}$$

The space derivative of the added mass term f(x) is

$$\frac{0.64}{2}\ \rho\frac{4}{3}\pi 3x^2 \qquad \text{(B-9)}$$

Substituting the appropriate terms into the equation for the acceleration of the sphere, we have

$$\frac{d^2y}{dt^2} = \frac{-1.28\rho\pi V_o\ x(r - y)dy/dt}{\left[1 + \frac{0.64}{2}\frac{\rho\pi}{m}\frac{4}{3}x^3\right]^2} \qquad \text{(B-10)}$$

If the sphere, as in our case, is taken to be aluminum (0.100 lbs./in.^{3}) and the fluid is water (62.4 lbs./ft.^{3}), for a 2-inch-diameter sphere, we have

$$\frac{d^2y}{dt^2} = -V_o\ \frac{(0.345)x(1-y)dy/dt}{\left[1 + 0.115x^3\right]^2} \qquad \text{(B-11)}$$

where the dimensions of x and y are in inches and time is in seconds. It would have been possible to find the force

on the sphere directly from the above equation (i.e., $F = m\ddot{y}$) if one were to assume that dy/dt were constant throughout the motion of the sphere through the water surface. Instead, a finer approximate solution will result if the velocity of the sphere is corrected at each point the calculation of the acceleration is made. This was done for the case of the 2-inch-diameter aluminum sphere entering the water normally at a velocity of 28 feet per second.

Increments of the vertical distance y were taken at 0.010 inch. At each point the variable x was calculated from the geometric relationships previously described. Over the first increment, the acceleration was calculated using the values of x, y, V_o and dy/dt. The value of dy/dt over the first increment is, of course, V_o. The time to the end of the first increment is given as the ratio of the distance increment to the velocity over that increment. The value of the acceleration just calculated is used to correct the velocity for the beginning of the second increment. The change of velocity over the first increment is given as the integral of the product of the acceleration and the time. In this case, it is the product of the acceleration and the time increment. This value of the change of velocity is subtracted from the original velocity to give the new corrected velocity to be used at the beginning of the second increment.

The above procedure was repeated for 61 such increments of distance. After this point the calculations were terminated, since the flow around the sphere separates and the added mass approximation for the momentum theorem is no longer valid. This separation point occurs at approximately 67 degrees up the side of the sphere and can be seen from the photographs and line drawing of the water-entry cavity.

After the values of the acceleration were calculated, the standard impact drag coefficient curve was plotted by use of the following relationship:

$$C_D = \frac{-2m\ddot{y}}{\rho A V_o^2} \qquad \text{(B-12)}$$

where C_D = impact drag coefficient

m = mass of the sphere

ρ = density of the fluid

A = maximum cross-sectional area of the sphere

V_o = initial entrance velocity of the sphere.

This curve has been plotted and compared with two of Shiffman's and Spencer's theoretical drag coefficient curves and one of Mosteller's experimental curves. The agreement is very good except for a slight positive shift in time of the results of the momentum equation.

Pressure Results from the Momentum Equation. The equation for the acceleration of the sphere as it traverses through the water surface allows one to find the axial force on the sphere: thus,

$$F = m\ddot{y} = V_o\left[1 + \frac{f(x)}{m}\right]^{-2} \frac{df(x)}{dx}\frac{dx}{dt}$$

$$F = \frac{-V_o}{\left[1 + 0.115x^3\right]^2} \frac{0.64}{2}\frac{4}{3}\rho 3x^2\pi\left(\frac{1-y}{x}\right)\frac{dy}{dt} \qquad \text{(B-13)}$$

An average impact pressure across the wetted area of the sphere could be defined as the total force on the sphere divided by the cross-sectional area of the sphere intersected by the plane water surface; i.e., πx^2. Then

$$\text{Pressure across the face of the sphere} = \frac{F}{\pi x^2}$$

$$= \frac{-V_o(1.2 \times 10^{-4})}{(1 + 0.115x^3)^2}\left(\frac{1-y}{x}\right)\frac{dy}{dt} \qquad \text{(B-14)}$$

where distances are measured in inches, time is measured in seconds, and pressure in psi.

The pressure has been calculated at each of the 61 points previously mentioned and plotted as a function of time.

It is easily seen that the pressure across the face of the sphere at time $t = 0$ is undefined in the above equation. The large value of pressure is due to the supersonic rate of growth of the wetted area of the sphere (reference (15)), and will assume a finite value due to the compressibility of the water. An approximate value of this pressure can be calculated in the following manner, due to von Karman. When the sphere first contacts the flat water surface, pressure is

propagated at the nose with the local speed of sound, c_1. The mass of fluid accelerated in a small time, dt, across a small area of the nose, dA, is given by $\rho c_1 dA\, dt$. The velocity of this mass of fluid was increased from zero to V_o in the time dt; hence, the small force acting on this mass is $dF = \rho c_1 dA dt \frac{V_o}{dt} = \rho c_1 V_o dA$. The pressure across the nose is then given by $dF/dA = \rho c_1 V_o$.

APPENDIX C

DERIVATION OF THE HYDRODYNAMIC PRESSURES RESULTING FROM HALF-BODY FLOW THEORY

If the formation of the cavity, as produced by the entrance of a sphere into water, is stopped on high-speed motion-picture film, a resemblance is seen between the cavity shape and that of a half-body in a moving fluid.

The shape of the half-body and the resulting pressure field can be derived in the following manner.

The velocity potential for a source of strength m located at the origin is,

$$\Phi = \frac{m}{4\pi r}$$

The velocity potential for a uniform stream of fluid having a velocity U in the negative x direction is,

$$\Phi = Ur \cos \theta \qquad \text{(C-1)}$$

The uniform flow and the source flow may be combined by adding the two velocity potential functions,

$$\Phi = \frac{m}{4\pi r} + Ur \cos \theta \qquad \text{(C-2)}$$

The stream function and the velocity potential are related in the following way in spherical polar coordinates:

$$\frac{\partial \psi}{\partial r} = -\sin \theta \frac{\partial \Phi}{\partial \theta}$$

$$\frac{\partial \psi}{\partial \theta} = r^2 \sin \theta \frac{\partial \Phi}{\partial r} \qquad \text{(C-3)}$$

Using these relationships, it is easy to show that the stream function is given by

$$\psi = \frac{m}{4\pi} \cos \theta + \frac{Ur^2}{2} \sin^2 \theta \qquad \text{(C-4)}$$

The stagnation point on the body is that point where the fluid velocity is zero with respect to the body. Hence, the velocity components of the fluid must be zero at that point, and

$$v_r = \frac{-\partial \phi}{\partial r} = 0, \quad v_\theta = \frac{-1}{r} \frac{\partial \phi}{\partial \theta} = 0 \tag{C-5}$$

which leads to

$$\frac{m}{4\pi r^2} - U \cos \theta = 0, \quad U \sin \theta = 0 \tag{C-6}$$

hence

$$\theta = 0 \quad \text{and} \quad r = \sqrt{\frac{m}{4\pi U}} = r_s \tag{C-7}$$

which are the coordinates of the stagnation point.

The value of the stream function which goes through the stagnation point is then $\psi_s = \frac{m}{4\pi}$, and hence the equation of the stream surface is

$$\cos \theta + \frac{2\pi U}{m} r^2 \sin^2 \theta = 1$$

$$\text{or} \quad r = \sqrt{\frac{m}{2\pi U} \frac{1 - \cos \theta}{\sin^2 \theta}} \times \sqrt{\frac{2}{2} \frac{1 + \cos \theta}{1 + \cos \theta}}$$

$$r = \frac{1}{2} \sqrt{\frac{m}{\pi U}} \sqrt{\frac{2}{1 + \cos \theta}} \tag{C-8}$$

$r = 1/2 \sqrt{\frac{m}{\pi U}} \sec \frac{\theta}{2}$ which is the equation of the half-body in the uniform flow.

Let the radius of a circular section of the half-body be denoted by $y(r, \theta) = r \sin \theta$. When this is substituted into the equation for the half-body surface,

$$\cos \theta + \frac{2\pi U}{m} r^2 \sin^2 \theta = 1 \tag{C-9}$$

the radius at that circular section is found to be

$$Y^2 = (1 - \cos\theta)\frac{m}{2\pi U} \tag{C-10}$$

The maximum value of the radius occurs at $\theta = \pi$, and its value is

$$Y_{MAX} = \sqrt{\frac{m}{\pi U}} \tag{C-11}$$

The dynamic pressure (pressure intensity) at any point is given by $\Delta p = \frac{\rho}{2}(U^2-q^2)$ where q is the total velocity of the fluid at the point. Hence,

$$q^2 = \left(\frac{\partial\phi}{\partial r}\right)^2 + \left(\frac{1}{r}\frac{\partial\phi}{\partial\theta}\right)^2 = U^2 + \frac{m^2}{16\pi^2 r^4} - \frac{mU\cos\theta}{2\pi r^2}$$

and

$$\Delta p = \frac{\rho U^2}{2}\left[\frac{m\cos\theta}{2\pi r^2 U} - \frac{m^2}{16\pi^2 r^4 U^2}\right] \tag{C-12}$$

In order to match the cavity produced by spheres entering water to that of a half-body shape, the curvature of the noses of the two shapes must be almost identical; i.e., the radius to the stagnation point of the half-body must equal the radius of the sphere.

Hence,

$$r_{sphere} = r_s = \sqrt{\frac{m}{4\pi U}} \tag{C-13}$$

and the equation of the stream surface is then

$$r = r_s \sec\frac{\theta}{2} \tag{C-14}$$

The pressure equation then becomes

$$\frac{\Delta p}{1/2\rho U^2} = 2\left(\frac{r_s}{r}\right)^2\cos\theta - \left(\frac{r_s}{r}\right)^4 \tag{C-15}$$

The half-body shape has been plotted by letting the radius to the stagnation point equal one inch. This has been plotted on an outline of the shape of the cavity produced by a 2-inch-diameter sphere entering water vertically. As can be seen from the common plot, the comparison of the two shapes is very good. The worst disagreement occurs at the nose of the cavities where the actual cavity produced by the sphere is more pointed than that predicted by the half-body approximation.

Since good agreement was obtained between the half-body shape and the actual shape of the cavity produced by the sphere, one would expect to obtain similar agreement between pressures predicted by the half-body equation and those as measured at some point in the fluid.

1. Pressure Around the Open Cavity. In the theory for the half-body approximation for the shape of the cavity produced by a sphere at water entry, an equation is given for the pressure at any point in the fluid.

By means of this equation one can determine the pressure at any point along a line that is parallel to the path traveled by the sphere. In an effect, this simulates the passing by the pressure gage of the cavity produced by a sphere entering water.

The value of the velocity used in this equation is the velocity of the free-stream flow, or in the case of the transposed motion, the velocity of the sphere through the stagnant fluid.

In the actual case, after the sphere enters the water surface the velocity does not remain constant but suffers a continual attrition due to the drag on the sphere. Hence, in the pressure equation, the velocity must be corrected to a lower value as the sphere travels along its path. The correction may be found in the following manner: In the open cavity phase, the only force that is acting on the sphere, neglecting gravity, is the hydrodynamic drag. In this case the drag coefficient is given fairly accurately by the value of 0.30. Hence, the motion of the sphere after water-entry impact may be described by the usual differential equation

$$M\ddot{y} = -1/2\rho C_D A\dot{y}^2 \qquad \text{(C-16)}$$

the solution of which is, in velocity-distance variables,

$$\frac{V}{V_0} = e^{-\frac{1}{2m}\rho C_D A x} \tag{C-17}$$

The instantaneous velocity of the sphere may be calculated and plotted as a function of the distance traveled by the sphere. This new velocity is then substituted into the equation for the pressure, thus giving a more accurate description of the pressure felt at a point in the fluid as the cavity produced by the sphere passes by.

2. Pressure in the Cavity. The maximum value of the radius of a cross section of the half-body was found in the preceding section to be, at $\theta = \pi$

$$Y_{MAX} = \sqrt{\frac{m}{\pi U}} \tag{C-18}$$

For the case of the half-body cavity produced by a 2-inch-diameter sphere, then the theoretical maximum radius of the cavity is

$$Y_{MAX} = 2 \text{ inches} \tag{C-19}$$

Thus, if a pressure gage were placed between one and two inches away from the trajectory of a 2-inch-diameter sphere traveling underwater (as in our present case), the pressure gage would be inside the cavity after the sphere passed by.

APPENDIX D

BUBBLE OSCILLATION THEORY

After the water-entry cavity closes, whether it is a point, line, or base closure, the area of closure starts to move towards the model and forms a closed cavity of semi-elliptical shape around the model. This bubble (the closed cavity) seems to move with the model at a relatively constant velocity, pulsating in volume as it does so.

The bubble may be approximated as a spherical mass of air pulsating in an infinite fluid, the surrounding water being the inert mass which is set into vibration while the air in the bubble is contributing to the elasticity of the system.

The following derivation of the frequency of the pulsating bubble may be derived in an elementary way, due to Minnaert in his article on "musical air-bubbles," ref. (3).

In the theory of the derivation, the maximum potential energy accumulated during the compression of the bubble is set equal to the kinetic energy of the water particles when the bubble is at its equilibrium volume.

Let the radius of the bubble oscillate according to the law, $r = r_o + a \sin \frac{2\pi t}{T}$

where r = the instantaneous radius of the bubble

r_o = equilibrium radius of the bubble

a = the maximum deviation of the radius of the bubble from its equilibrium value

T = period of oscillation of the bubble.

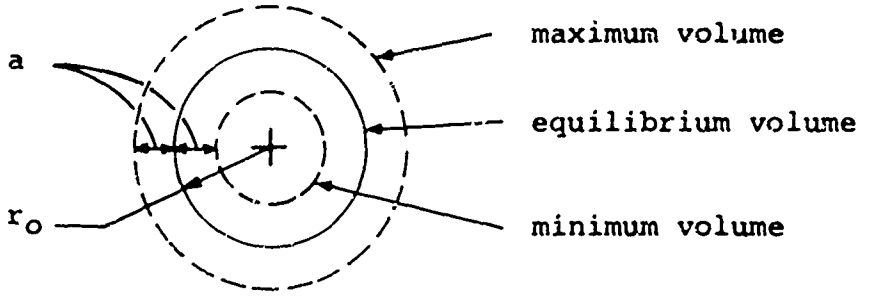

When the radius of the bubble has decreased by a distance x, the volume of the bubble has decreased in the proportion

$$\left(\frac{r_o - x}{r_o}\right)^3 \tag{D-1}$$

If the compression of the air in the bubble is adiabatic, for which $C_p/C_v = k$, the pressure will now be given by

$$\frac{p}{p_o} = \left(\frac{V_o}{V}\right)^k = \left(\frac{r_o}{r_o - x}\right)^{3k} \tag{D-2}$$

This may be written as

$$\frac{p_o}{p} = \left(1 - \frac{x}{r_o}\right)^{3k}$$

By the binomial expansion theorem

$$(1 - y)^n = 1 - ny + \text{---}, \quad y^2 < 1 \tag{D-3}$$

the pressure ratio equation may be written as

$$p - p_o = 3kp\frac{x}{r_o} \tag{D-4}$$

which is the excess of the pressure inside the cavity over the pressure outside the cavity, the value always being a small fraction of the normal, or equilibrium pressure.

The potential energy at minimum volume is

$$-\int_{V_o}^{V} (p-p_o)\,dv = \int_o^a \frac{3kpx}{r_o} 4\pi r_o^2 \,dx = 6\pi kpra^2 \tag{D-5}$$

The kinetic energy of the water particles is determined by the motion of the fluid around the bubble, which for symmetry reasons is directed radially.

The velocity of the wall of the bubble is

$$\frac{dr}{dt} = \frac{2\pi a}{T} \cos \frac{2\pi t}{T} \tag{D-6}$$

while the velocity of a particle of water at a distance R from the origin of the bubble is

$$\frac{r_o^2}{R^2} \frac{2\pi a}{T} \cos \frac{2\pi t}{T} \tag{D-7}$$

At the time t = 0, the particles of water have their maximum velocities, $\frac{r_o^2}{R^2} \frac{2\pi a}{T}$, and the total kinetic energy of the system is then,

$$1/2 \int \left(\frac{dr}{dt}\right)^2_{MAX} dm = \frac{\rho}{2} \int_{r_o}^{\infty} \frac{r_o^4}{R^4} \frac{4\pi^2 a^2}{T^2} 4\pi R^2 dR$$

$$= \frac{8\pi^3 \rho r_o^3 a^2}{T^2} \tag{D-8}$$

where ρ is the density of the water. The kinetic energy of the air inside the bubble is neglected since this is small compared to the total kinetic energy. The integration is carried to the limit ∞ since the bubble is assumed to be surrounded by a very great volume of water.

Equating the expression for the maximum potential energy of the compression of the bubble equal to the maximum kinetic energy of the surrounding fluid, the period and frequency of the bubble are found to be:

$$T^2 = \frac{4\pi^2 \rho r_o^2}{3kp}, \quad f = \frac{1}{2\pi r_o} \sqrt{\frac{3kp}{\rho}} \tag{D-9}$$

The frequency of oscillation of the bubble is inversely proportional to the equilibrium radius of the bubble for any bubble at any given point in the fluid.

UNCLASSIFIED

Security Classification

DOCUMENT CONTROL DATA - R & D

Security classification of title, body of abstract and indexing annotation must be entered when the overall report is classified

1 ORIGINATING ACTIVITY (Corporate author) U. S. Naval Ordnance Laboratory White Oak, Silver Spring, Maryland	2a. REPORT SECURITY CLASSIFICATION UNCLASSIFIED 2b. GROUP

3 REPORT TITLE

HYDRODYNAMIC PRESSURE MEASUREMENTS OF THE VERTICAL WATER ENTRY OF A SPHERE

4 DESCRIPTIVE NOTES (Type of report and inclusive dates)

5 AUTHOR(S) (First name, middle initial, last name)

William R. Hoover and
Victor C. D. Dawson

6 REPORT DATE 26 October 1966	7a. TOTAL NO OF PAGES 62	7b. NO OF REFS 15
8a. CONTRACT OR GRANT NO b. PROJECT NO c. d.	9a ORIGINATOR'S REPORT NUMBER(S) NOLTR 66-70 9b. OTHER REPORT NO(S) (Any other numbers that may be assigned this report) Ballistics Research Report 161	

10 DISTRIBUTION STATEMENT

Distribution of this document is unlimited

11. SUPPLEMENTARY NOTES	12 SPONSORING MILITARY ACTIVITY

13 ABSTRACT

The phenomena associated with the vertical water entry of 2-inch-diameter aluminum spheres striking the water surface at 28 feet per second have been investigated by the use of hydrophones placed below the water surface.

The pressure recordings from the hydrophones have been analyzed for the three distinct phases of the water-entry problem: namely, (1) impact phase, (2) cavity flow phase, and (3) cavity collapse.

DD FORM 1 NOV 68 1473 (PAGE 1)

S/N 0101-807-6801

UNCLASSIFIED

Security Classification

UNCLASSIFIED

Security Classification

14 KEY WORDS	LINK A		LINK B		LINK C	
	ROLE	WT	ROLE	WT	ROLE	WT
water entry						
sphere						
impact forces						
cavity flow						
cavity collapse						
cavity oscillation						
hydrodynamic drag						
dipole theory						
half-body theory						
bubble formation						
bubble oscillation						
hydrodynamic instrumentation						
pressure measurements						
potential flow						
optical measurements						
hydrodynamic pressure						

DD FORM 1 NOV 65 1473 (BACK)

(PAGE 2)

UNCLASSIFIED

Security Classification